







Review

A Comprehensive Review on the Conventional and Non-Conventional Machining and Tool-Wear Mechanisms of INCONEL[®]

A. F. V. Pedroso ¹, V. F. C. Sousa ¹, N. P. V. Sebbe ¹, F. J. G. Silva ^{1,2,*}, R. D. S. G. Campilho ^{1,2},
R. C. M. Sales-Contini ^{1,3} and A. M. P. Jesus ^{2,4}

¹ ISEP, Polytechnic Institute of Porto, R. Dr. António Bernardino de Almeida, 4249-015 Porto, Portugal

² Associate Laboratory for Energy, Transports and Aerospace (LAETA-INEGI), Rua Dr Roberto Frias, 400, 4200-465 Porto, Portugal

³ Aeronautical Structures Laboratory, Faculdade de Tecnologia de São José dos Campos Prof. Jessen Vidal, Centro Paula Souza, São José dos Campos, 1350 Distrito Eugênio de Melo, São José dos Campos 12247-014, SP, Brazil

⁴ Faculty of Engineering, Department of Mechanical Engineering, University of Porto, Rua Dr. Roberto Frias, 400, 4200-465 Porto, Portugal

* Correspondence: fgs@isep.ipp.pt; Tel.: +351-228340500

Abstract: Nickel-based superalloys, namely INCONEL[®] variants, have had an increase in applications throughout various industries like aeronautics, automotive and energy power plants. These superalloys can withstand high-temperature applications without suffering from creep, making them extremely appealing and suitable for manufactured goods such as jet engines or steam turbines. Nevertheless, INCONEL[®] alloys are considered difficult-to-cut materials, not only due to their superior material properties but also because of their poor thermal conductivity (k) and severe work hardening, which may lead to premature tool wear (TW) and poor final product finishing. In this regard, it is of paramount importance to optimise the machining parameters, to strengthen the process performance outcomes concerning the quality and cost of the product. The present review aims to systematically summarize and analyse the progress taken within the field of INCONEL[®] machining sensitively over the past five years, with some exceptions, and present the most recent solutions found in the industry, as well as the prospects from researchers. To accomplish this article, ScienceDirect, Springer, Taylor & Francis, Wiley and ASME have been used as sources of information as a result of great fidelity knowledge. Books from Woodhead Publishing Series, CRC Press and Academic Press have been also used. The main keywords used in searching information were: “Nickel-based superalloys”, “INCONEL[®] 718”, “INCONEL[®] 625” “INCONEL[®] Machining processes” and “Tool-wear mechanisms”. The combined use of these keywords was crucial to filter the huge information currently available about the evolution of INCONEL[®] machining technologies. As a main contribution to this work, three SWOT analyses are provided on information that is dispersed in several articles. It was found that significant progress in the traditional cutting tool technologies has been made, nonetheless, the machining of INCONEL[®] 718 and 625 is still considered a great challenge due to the intrinsic characteristics of those Ni-based-superalloys, whose machining promotes high-wear to the tools and coatings used.

Keywords: nickel-based superalloys; INCONEL[®] 718; INCONEL[®] 625; INCONEL[®] machining processes and tool-wear mechanisms



Citation: Pedroso, A.F.V.; Sousa, V.F.C.; Sebbe, N.P.V.; Silva, F.J.G.; Campilho, R.D.S.G.; Sales-Contini, R.C.M.; Jesus, A.M.P. A Comprehensive Review on the Conventional and Non-Conventional Machining and Tool-Wear Mechanisms of INCONEL[®]. *Metals* **2023**, *13*, 585. <https://doi.org/10.3390/met13030585>

Academic Editor: Yadir Torres Hernández

Received: 14 February 2023

Revised: 2 March 2023

Accepted: 9 March 2023

Published: 13 March 2023



Copyright: © 2023 by the authors. Licensee MDPI, Basel, Switzerland. This article is an open access article distributed under the terms and conditions of the Creative Commons Attribution (CC BY) license (<https://creativecommons.org/licenses/by/4.0/>).

1. Introduction

With the increasing requirement to achieve the best thermal efficiency in the field of aeronautics [1,2] and energy power plants steam turbines [3], applications in which aluminium and steel would succumb to creep [4] as a result of thermally induced crystal

vacancies [5], nickel-based (Table 1) alloys became a very attractive solution for high-temperature operation [6–9]. Ni-Cr-Fe superalloys (Figure 1, blue zone), better known as INCONEL[®] (trademark registered by the International Nickel Company of Delaware and New York [10]), are materials resistant to oxidation, caustic and high-purity water corrosion, and stress-corrosion cracking (SCC) [11], optimal for service in extreme environments subjected to high mechanical loads [12], within numerous applications and characteristics (Table 2).

Table 1. Some physical properties of nickel (adapted from [7]).

Characteristic		Value	Units
Z		58.71	AMU
Crystal structure		FCC	[-]
Lattice constant	@ 25 °C	0.35238	nm
ρ		8908	kg/m ³
T_m		1453	°C
T_C		353	
c_p		0.44	kJ/kg K
α		13.3×10^{-6}	K ⁻¹
	@ 100 °C	82.8	
k	@ 300 °C	63.6	W/m K
	@ 500 °C	61.9	
ρ_R	@ 20 °C	6.97×10^{-8}	Ωm
B_{max}		0.617	T
B_r		0.300	
H_C		239	A/m
E		206.0	GPa
G		73.6	
ν		0.30	[-]

Caption: B_{max} —saturation magnetization; B_r —residual magnetization; c_p —specific heat at constant pressure; E —Young's Modulus; FCC—face-centred cubic; G —shear modulus; H_C —coercive force; T_C —Curie temperature; T_m —melting temperature; Z —atomic mass; α —thermal expansion coefficient; ρ —volumetric mass density; ρ_R —electrical resistivity, ν —Poisson's coefficient.

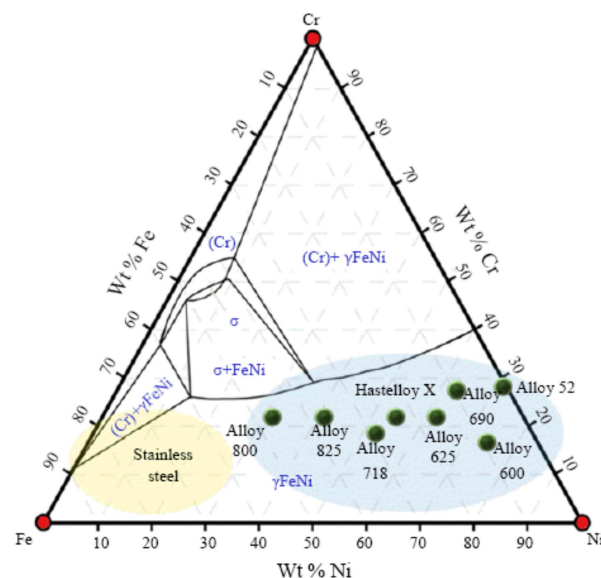


Figure 1. Fe-Ni-Cr ternary phase diagram [13] (Caption: wt%—element weight percentage).

A brief insight is provided with the most known alloys, including the INCONEL[®] 600, a Ni-Cr alloy that offers high levels of resistance to several corrosive elements. In high-temperature situations, INCONEL[®] 600 will not succumb to Cl-ion SCC or general oxidation, but it can still undergo corrosion by sulphuration deterioration in the high-

temperature flue gas. This was a research topic by Wei, et al. [14]. INCONEL[®] 600 also suffers from severe hydrogen embrittlement at 250 °C [15]. Nonetheless, this alloy is recommended for use in furnace components and chemical processing equipment [16]. Moreover, INCONEL[®] 600 is also effectively used in the food industry and nuclear engineering due to its constant crystalline structure in applications that would cause permanent distortion to other alloys [17].

Table 2. Summary of applications and characteristics of some nickel-based superalloys (adapted from [18,19]).

Superalloy	Sub-Grouped Material	Industry Applications	Characteristics
Ni-based alloys	INCONEL [®] (587, 597, 600, 601, 617, 625, 706, 690, 718, X750, 901)	Aircraft motors, nuclear reactors, gas turbines, spacecraft, pumps, furnaces, heat-treating equipment, petrochemical processing equipment, chemical processing, submarine, and manufacturing industry.	600: Solid solution strengthened; 625: Acid resistant, good weldability; 690: Low cobalt content for nuclear applications, and low resistivity; 718: Gamma phase (γ') double prime solution strengthened with good weldability.
	INCONEL [®] 722	Acids in the chemical industry	-
	INCONEL [®] 751	-	Increased Al content for improved failure strength in the 870 °C range. Increased Al content for improved
	INCONEL [®] 792	-	high-temperature corrosion properties, especially used in gas turbines.
	INCONEL [®] 903	Petrochemical tubing.	-
	INCONEL [®] 939	-	γ' prime strengthened with good weldability.

The INCONEL[®] 601 alloy, similarly to INCONEL[®] 600, resists various forms of high-temperature corrosion and oxidation [20]. Nevertheless, this Ni-Cr alloy has an addition of aluminium which results in higher mechanical properties, even in extremely hot environments. INCONEL[®] 601 can prevent the significant strains (ϵ) that would appear under operating loads when exposed to high-temperature environments. The applications go from the use in furnaces to heat-treating equipment like retorts, baskets and gas-turbine components [21] to petrochemical processing equipment. The INCONEL[®] 625, which will have a special focus during this study, is a rare alloy that gains strength without having to undergo an extensive strengthening heat treatment [22]. It is a Ni-Cr-Mo alloy with an addition of Nb. The Nb reacts with Mo, causing the alloy's matrix to stiffen and increase its strength [23]. Like most INCONEL[®] alloys, the INCONEL[®] 625 has high resistance to several corrosive elements [24], withstanding harsh environments that would severely affect the performance of other alloys. This alloy is particularly effective when it comes to staving-off crevice corrosion and pitting. The INCONEL[®] 625 is a versatile alloy that is effectively used in the marine engineering, aerospace, chemical, and energy industries, among other applications [25,26]. The INCONEL[®] 690 alloy, unlike others in the group, is a high Ni and Cr alloy (Cr gives it particularly strong resistance to corrosion [15,27] that occurs in aqueous atmospheres). Along with its ability to resist the corrosion caused by oxidizing acids and salts, INCONEL[®] 690 can also withstand the sulfidation that takes place at

extremely high temperatures (T). One of the most known INCONEL[®] alloys is the 718 alloy. This alloy, along with the formerly mentioned 625 alloy, will also have a special focus. INCONEL[®] 718 differs from other INCONEL[®] variants in structure and response, since it is designed for operation at $T \leq 650$ °C [28]. The 718 alloy is obtained by precipitation hardening [29,30]. It contains substantial levels of Fe, Mo, and Nb, as well as trace amounts of Ti and Al [31]. It has good weldability, which is not matched by most INCONEL[®] alloys [32], and combines anti-corrosive elements with a high level of strength and flexibility. It is particularly resistant to post-weld cracking, maintaining its structure in both high-temperature and aqueous environments as well, being most widely used in different industries, such as petrochemical, aeronautics, energy, and aerospace [33]. INCONEL[®] alloys tend to form a thick and stable passivating oxide layer to protect the surface from further attack, retaining strength over a wide T range, making INCONEL[®] an attractive material for high-temperature applications [34]. The strength at high-temperatures of INCONEL[®] alloys may be developed by solid solution strengthening or precipitation strengthening, depending on the alloy [35]. In those processes, small amounts of niobium combine with nickel to form the intermetallic compound Ni_3Nb or γ -prime, which consists of small cubic crystals that inhibit slip and creep effectively at elevated T [36].

Concerning the roles of major phases or composition elements that contribute to the INCONEL[®] alloys, an overview is presented in Table 3 on the effects of Ni-alloying to better comprehend the compositions presented in Table 4.

Table 3. Major roles of solutes in different types of INCONEL[®] alloys [26].

Element	Fe-Base	Co-Base	Ni-Base
Cr	Improves hot corrosion and oxidation resistance. Solid-solution hardening.	M_{23}C_6 and M_7C_3 carbide precipitation (M_xC_y metallic carbide). Improves hot corrosion and oxidation resistance. Promotes Topologically Close-Packed (TCP) phases, also called Frank–Kasper phases.	M_{23}C_6 and M_7C_3 carbide precipitation. Improves hot corrosion and oxidation resistance. Moderate solid-solution hardening. A moderate increase in γ' volume fraction ($vt\%$). Tends to stabilize the Ni_2Cr phase in alloys containing more than 20% Cr. Promotes TCP phases.
Al	Induces γ' precipitation. Retards formation of hexagonal η - Ni_3Ti phase.	Improves oxidation resistance. Forms intermetallic β -CoAl.	Moderate solid-solution hardening. Induces γ' precipitation. Improves oxidation resistance. Moderate solid-solution hardening.
Ti	γ' precipitation. TiC carbide precipitation.	TiC carbide precipitation. Formation of Co_3Ti intermetallic. Formation of Ni_3Ti with sufficient Ni. Reduces surface stability.	γ' precipitation. TiC carbide precipitation. Retards the precipitation of $\text{Ni}_2(\text{Cr}, \text{Mo})$ phase particles. High solid-solution hardening.
Mo	Solid solution hardening. Forms M_6C carbide precipitates.	Solid solution hardening. Forms Co_3Mo intermetallic precipitates. Promotes TCP phases.	A moderate increase in γ' $vt\%$. M_6C and MC carbide formation. Promotes formation of $\text{Ni}_2(\text{Cr}, \text{Mo})$ phase particles. Promotes σ and μ -TCP phases. High-solid solution hardening.
W	Solid solution hardening. M_6C carbide precipitation.	Solid solution hardening. Formation of Co_3W intermetallic. Promotes TCP phases.	A moderate increase in γ' $vt\%$. M_6C carbide formation. Increases ρ . Promotes the formation of $\text{Ni}_2(\text{Cr}, \text{Mo}, \text{W})$ particles. Promotes σ and μ -TCP phases.
Ta	γ'' precipitation. Forms TaC carbide precipitates.	M_6C and MC carbide precipitation. Formation of Co_2Ta intermetallic. Reduces surface stability.	High-solid solution hardening. TaC carbide precipitation. A large increase in γ' $vt\%$. Improves oxidation resistance.

Table 3. Cont.

Element	Fe-Base	Co-Base	Ni-Base
Nb	γ'' precipitation. NbC carbide precipitation. δ -Ni ₃ Nb precipitation.	M ₆ C and MC carbide precipitation. Formation of Co ₂ Nb intermetallic. Reduces surface stability.	High-solid solution hardening. A large increase in γ' vol%. NbC carbide formation. γ'' precipitation. δ -Ni ₃ Nb precipitation. Moderate solid-solution hardening.
Re	-	-	Increases γ/γ' lattice mismatch. Retards coarsening. Decreases oxidation resistance.
Fe	Not applicable.	Improves workability.	Promotes σ and Laves TCP phases. Improves workability.
Co	-	Not applicable.	Raises γ solidus T . A moderate increase in γ' vol% in some alloys. Raises γ' solvus T .
Ni	FCC matrix stabilizer. Inhibits TCP phase precipitation.	FCC stabilizer. Decreases hot corrosion resistance.	Not applicable.
C	Carbide formation. Stabilizes FCC matrix. Improves creep strength and ductility.	Carbide formation. Decreases ductility.	Carbide formation. Moderate solid-solution Hardening. Moderate solid-solution hardening.
B	Retards formation of grain-boundary η -Ni ₃ Ti Improves creep strength and ductility.	Improves creep strength and ductility	Inhibits carbide coarsening. Improves grain-boundary strength.
Zr	Retards formation of grain-boundary η -Ni ₃ Ti.	ZrC carbide formation. Improves creep strength and ductility. Reduces surface stability.	Improves creep strength and ductility. Moderate solid-solution hardening. Inhibits carbide coarsening.
Hf	-	-	Improves grain-boundary strength. Improves creep strength and ductility. HfC formation.
V	Improves notch ductility at elevated T . Improves hot workability.	-	Promotes eutectic γ/γ' formation. Imparts extra passivation to some alloys in certain liquid media.

Table 4. Chemical composition of relevant INCONEL® alloys.

INCONEL®	182 [37]	600 [38]	601 [39]	625 [40]	690 [38]	713C [41]	718 [42]	X750 [43]	800 [44]	825 [45]
Ni	62	Bal.	62.6	60.76	Bal.	71.76	53.98	71.32	35	38.25
Cr	15	15.2	23.05	21.69	29.9	12.7	18.11	16.22	23	22.70
Fe	Bal.	11.0	-	4.21	11.6	1.6	Bal.	8.04	39.5	31.08
Mo	-	-	-	8.62	-	4.6	3.00	-	-	2.77
Nb & Ta	2.0	-	-	3.38	-	2.2	5.44	0.9	-	-
Co	-	-	-	-	-	0.06	-	0.01	-	0.04
Mn	5.5	0.23	0.1	0.31	0.25	0.04	-	0.21	-	0.12
Cu	0.5	-	0.1	-	-	-	-	0.03	-	2.78
Al	-	-	1.4	0.53	-	5.9	0.53	0.68	0.15–0.6	0.05
Ti	1.0	0.3	-	0.21	0.3	0.71	1.01	2.47	0.15–0.6	0.65
Si	1.0	0.29	0.37	0.40	0.33	0.08	-	0.08	-	0.36
C	0.06	0.022	0.025	0.04	0.025	0.188	-	0.04	≤0.1	0.04
S	0.02	0.025	-	-	0.025	0.006	-	-	-	0.02
P	0.02	0.086	-	-	0.01	0.005	-	-	-	0.01
B	-	-	-	-	-	0.014	-	-	-	-
W	-	-	-	-	-	0.06	-	-	-	0.36
Zr	-	-	-	-	-	0.14	-	-	-	-
V	-	-	-	-	-	-	-	-	-	0.06
N	-	0.024	-	-	0.02	-	-	-	-	-

Caption: Bal.—Balance.

As it was possible to find out, some of the consequences of alloying Ni with certain chemical elements make INCONEL[®] alloys [46] a difficult-to-machine material [47] (Figure 2) and difficult to metal shape [48], identically to stainless steel [49,50]. As opposed to other alloys, like Al-alloys [36,51], Magnesium (Mg) alloys [51], steel alloys [52] or Ti-alloys [51], INCONEL[®] alloys do not benefit from better-established wear mechanisms between the pair tool-workpiece.

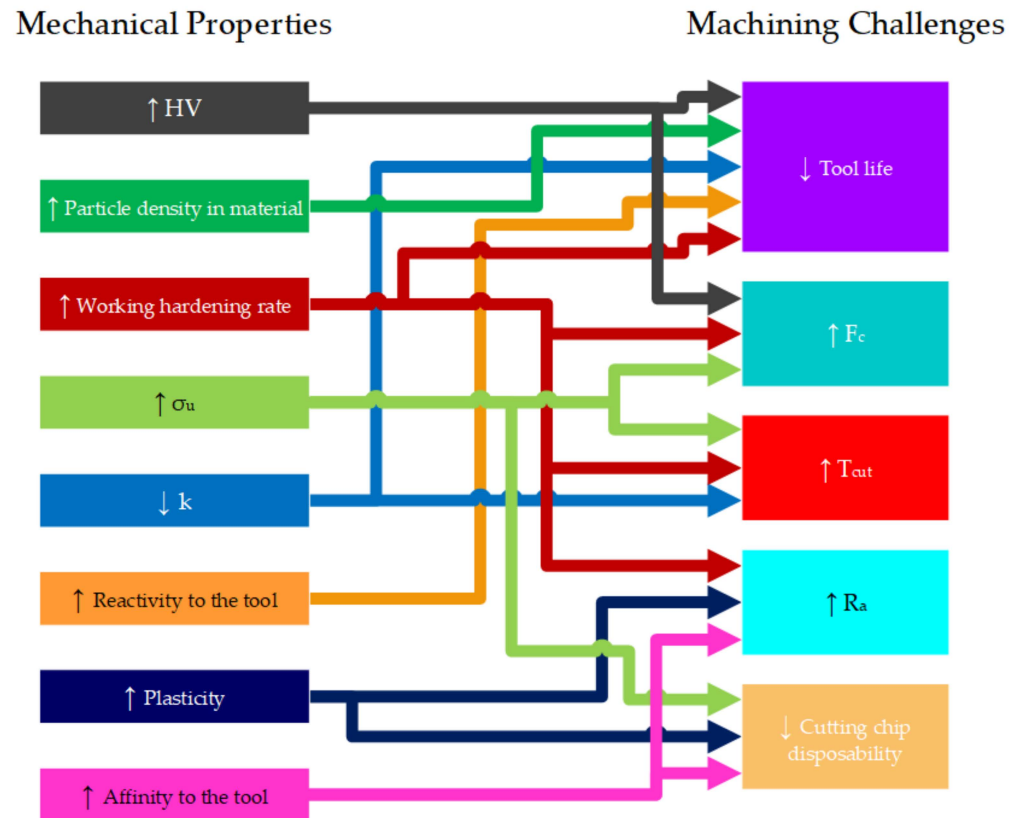


Figure 2. Relationship between mechanical properties and machining challenges with INCONEL[®] (adapted from [19]).

Table 5 presents the most relevant and used models of the better-established wear mechanisms referred to, based on physics and experiments for heat partition coefficient R_{chip} , for common materials like aluminium and low carbon mild steels.

Table 5. Predictive models based on physics and experiment for heat partition coefficient R_{chip} [53].

A Predictive Model for Heat Partition Coefficient R_{chip}	Equation	Establishment Basis
Loewen—Shaw [54]	$R_{L-SH} = \frac{q_F \cdot \frac{I_c}{\lambda_T} \cdot A - \Delta\theta_{p \max} + \theta_0}{q_F \cdot \frac{I_c}{\lambda_T} \cdot A + q_F \cdot \frac{0.377 \cdot I_c}{\lambda_W \cdot \sqrt{\frac{v_{ch} \cdot I_c}{4 \cdot a_W}}}}$	Dry-cutting process of AISI 1113 steel with K ₂ S cemented carbide tool (cutting speed, $v_c = 30\text{--}182$ m/min).
Shaw [55]	$R_{SH} = \frac{1}{1 + \left(0.754 \cdot \frac{\lambda_T}{\lambda_W}\right) / A \cdot \sqrt{\frac{v_{ch} \cdot I_c}{2 \cdot a_W}}}$	Dry-cutting process of AISI 1113 steel with high-speed steel (HSS) tool/K ₂ S cemented carbide tool ($v_c = 30\text{--}182$ m/min).
Kato—Fujii [56]	$R_{KF} = \frac{1}{1 + \frac{\lambda_T}{\lambda_W} \cdot \sqrt{\frac{a_W}{a_T}}}$	Surface grinding process of stainless steel/carbon steel with Al-oxide wheel.

Table 5. Cont.

A Predictive Model for Heat Partition Coefficient R_{chip}	Equation	Establishment Basis
List—Sutter [57]	$R_{L-SU} = \frac{1}{1 + 0.754 \cdot \frac{\lambda_T \cdot \sqrt{v_{ch} \cdot l_c}}{\lambda_W \cdot \sqrt{\alpha_W}} \cdot \frac{1}{\frac{2}{\pi} \cdot \left[\ln \left(\frac{2\alpha_W}{l_c} \right) + \frac{1}{3} \cdot \frac{l_c}{w} + \frac{1}{2} \right]}}$	Dry-cutting process of AISI 1018 mild steel with uncoated carbide tool ($v_c = 23\text{--}60$ m/min; undeformed chip thickness (h_{ch}) range 0.26–0.38 mm).
Gecim—Winer [58]	$R_{G-W} = \frac{0.807 \cdot \lambda_W \cdot \sqrt{\frac{v_{ch} \cdot l_c}{\alpha_W}}}{\lambda_T + 0.807 \cdot \lambda_W \cdot \sqrt{\frac{v_{ch} \cdot l_c}{\alpha_W}}}$	Based on the thermal behaviour of the two-dimensional, transient T distribution in the vicinity of a small, stationary, circular heat source equation of the average T of the moving and stationary heat sources between a frictional contact.
Reznikov [59]	$R_R = \frac{1}{1 + 1.5 \cdot \frac{\lambda_T}{\lambda_W} \cdot \sqrt{\frac{\alpha_W}{\alpha_T}}}$	Based on the Green function to analyse the chip deformation and friction work along the tool rake face.
Berliner—Krajnov [60]	$R_{B-K} = \frac{1}{1 + 0.45 \cdot \frac{\lambda_T}{\lambda_W} \cdot \sqrt{\frac{\pi \cdot \alpha_W}{v_{ch} \cdot l_c}}}$	
Tian—Kennedy [60]	$R_{T-K} = \frac{1}{1 + \frac{\lambda_T}{\lambda_W} \cdot \sqrt{\frac{1 + \frac{v_{ch} \cdot l_c}{\alpha_T}}{1 + \frac{v_{ch} \cdot l_c}{\alpha_W}}}}$	Consideration of Peclet numbers for the tool and workpiece materials in sliding tribological contact.

Caption: A —area shape factor; l_c —tool-chip contact length; q_F —frictional heat flux generated in SDZ; R_{chip} —heat partition coefficient into the moving chip from the secondary deformation zone (SDZ); v_{ch} —chip moving speed; α_T —tool thermal diffusivity; w —tool-chip contact area; α_W —workpiece thermal diffusivity; $\Delta\theta_{p \max}$ —maximum tool-chip interface temperature rise due to heat generation in PDZ; θ^0 —environment temperature; λ_T —tool thermal conductivity; λ_W —workpiece thermal conductivity.

It is suggested to consult the work of Zhao, et al. [53] to better understand the additional variables described in Table 5.

Figure 3 explains how superficial hardness is affected in INCONEL[®] alloys when machined after cold work processes, compared to some more stable materials like Cu, Al and mild steel. Machining (or surface) cold working may result from mechanical machining (milling, lathing, grinding) [61] or surface treatment (sandblasting, shot-peening), and may introduce residual tensile or compressive stresses into the surface of materials. Compressive stresses generated by shot-peening processes prevent the occurrence of stress corrosion cracks. In the case of plastic strain, tensile stresses appear instead, and the resulting stress levels may be extremely high [62]. A curious detail patent in Figure 3 is the similarity behaviour between INCONEL[®] 718 and 625 alloys after the 20% cold reduction.

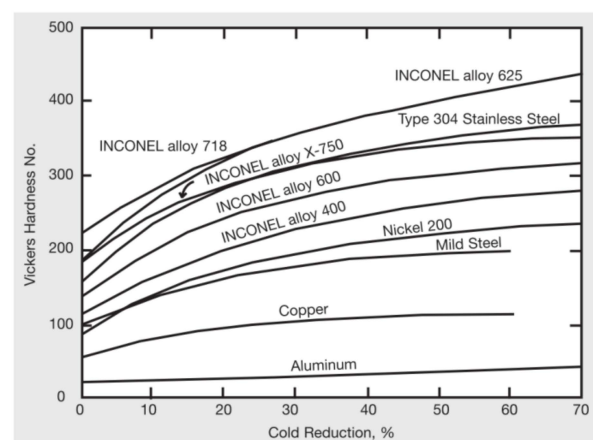


Figure 3. Effect of cold work on hardness for different INCONEL[®] alloys and comparison with other materials [1].

As a consequence of low k [36] of nickel-based alloys, which significantly influences heat distribution during the machining process, the surface integrity is affected when applying traditional cold forming techniques, due to the rapid work hardening (Figure 3) in the chip formation region [63]. This phenomenon leads to plastic deformation of either the INCONEL[®] workpiece or the tool, on subsequent machining passes [64], eventually resulting in built-up-edge (BUE) formation [31] (Figure 4) and consequentially in premature tool failure [65]. For this reason, age-hardened INCONEL[®] alloys, such as the 718 alloy, are typically machined using an aggressive but slow cut with a hard tool, minimizing the number of passes required [66].

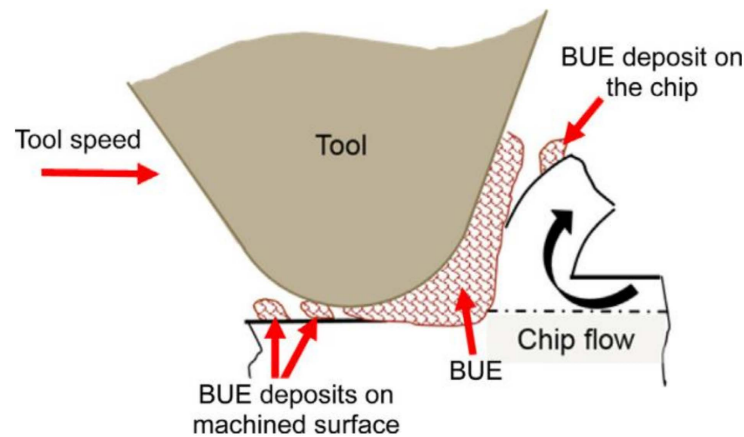


Figure 4. Schematic diagram of BUE formation in micromachining processes [67].

The BUE phenomenon occurs because of an accumulation of hot debris generated by the chip-start cutting process and deposited on the tool surface during machining, leading afterwards to adhesion and abrasion TW. From an experimental point of view, some authors noted that the BUE is significantly affected by the state of stress around the tool cutting edge and happens under extreme contact conditions at the tool–chip interface as high friction, high pressure, and high sliding velocity [68]. INCONEL[®] alloys are well known to abrade tools and develop BUE [69], especially the 718 alloy. Also during the machining of INCONEL[®] 625, heat concentration is likely to occur at the cutting edges, resulting in early tool failure and consequent BUE [70].

2. Method of Research

The research and information compiling method are illustrated in the flowchart of Figure 5, which is simple to visually interpret and track down all the inherent steps in the making of this specific paper. In the flowchart, all the consulted databases and most used keywords are found (in the topic of this document), to find information about conventional and non-conventional machining and tool-wear mechanisms of INCONEL[®] alloys.

Additionally, will be provided three attachments containing abbreviations, symbols and units used within the article.

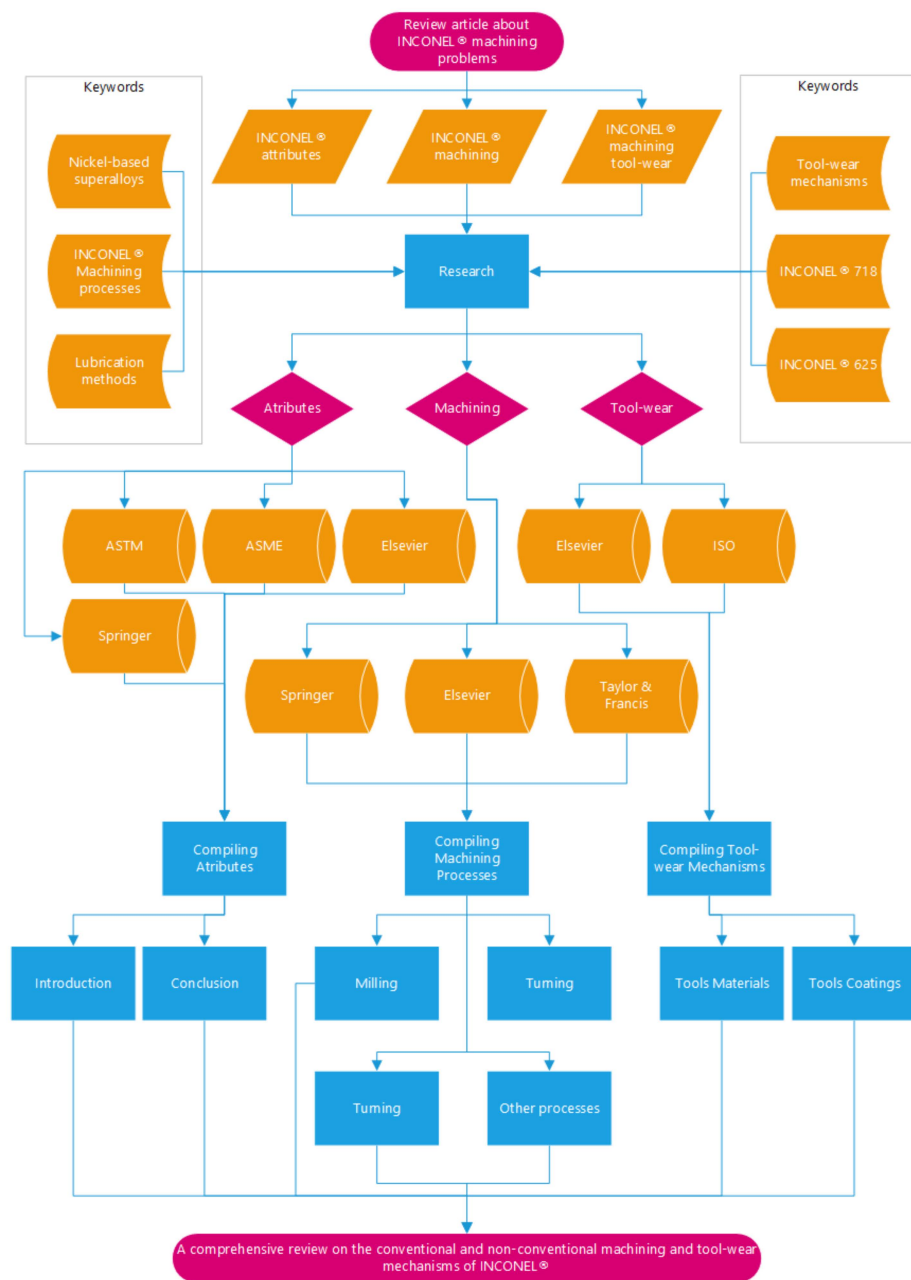


Figure 5. Research method accomplished to achieve a better redacting result to the review paper.

3. Literature Review

3.1. Conventional Manufacturing Processes

The machining process of chip-start cutting is a technological process able to transform a wrought stock into a component, using a cutting tool. The surplus material from the wrought stock, or just stock, is removed in the form of chips; a consequence of the mechanical action of a cutting wedge with higher hardness than the material of the component that is meant to manufacture. In the following literature review, Milling, Turning, Drilling and Boring will be the discussed processes, in which chip-start cutting is a key and common factor to all these traditional processes.

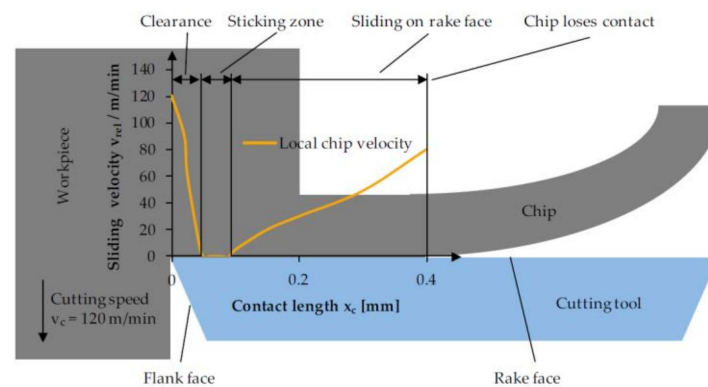


Figure 6. Evolution of the sliding velocity along the tool-material interface [71].

Making use of Figure 6, and taking into account that the chip-start cutting process is very much equal to the machining of INCONEL[®] 718 and 625, Bonnet et al. [72] described the different friction parts on the rake face in the machining of steel. Directly behind the cutting edge, the chip velocity rapidly shrinks to zero. For a certain contact length, the chip material has a sliding velocity of zero, which starts to increase for the rest of the tool-chip interface, before the chip loses contact with the tool [72].

Due to the friction created around the chip creation process, three distinct heat zones are created within the vicinities of the cutting wedge. In Figure 7, the three different thermal affected regions between the tool-workpiece are visible. In Figure 7a there is a thermo-mechanical deformation of the primary shear region (or primary deformation zone, PDZ) where the majority of the energy is converted into heat due to the internal friction of the material to be cut. In Figure 7b there is a tool-material interface region, or SDZ, of the tool rake surface and the chip rear face where heat is generated by the rubbing between the chip and the tool and finally. In Figure 7c the contact between the flank of the tool and the already machined surface takes place, called tertiary deformation zone (TDZ).

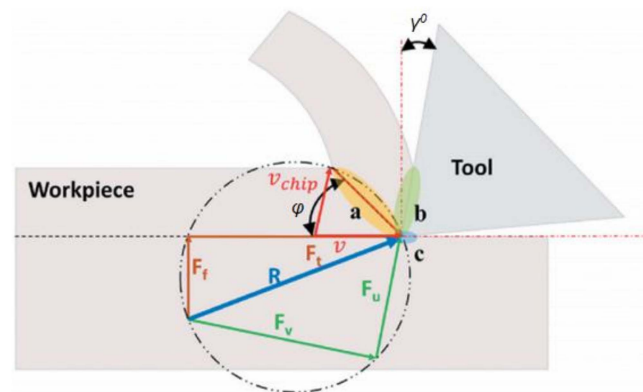


Figure 7. Regions of heat generation during metal orthogonal machining (adapted from [73]): (Caption: φ —shear plane angle; γ^0 —Rake angle, F_f —Feed force, F_t —tangential force).

A novel approach to improve the efficiency of the traditional chip-start cutting process is laser-assisted machining (LAM), illustrated in Figure 8, which consists of preheating the material to cut and lowering the superficial hardness to facilitate tool cutting. This solution is common to turning, milling and grinding. Kim and Lee [74] also worked on a machining preheat approach for the INCONEL[®] 718 alloy, which includes a magnetic induction coil instead of a laser.

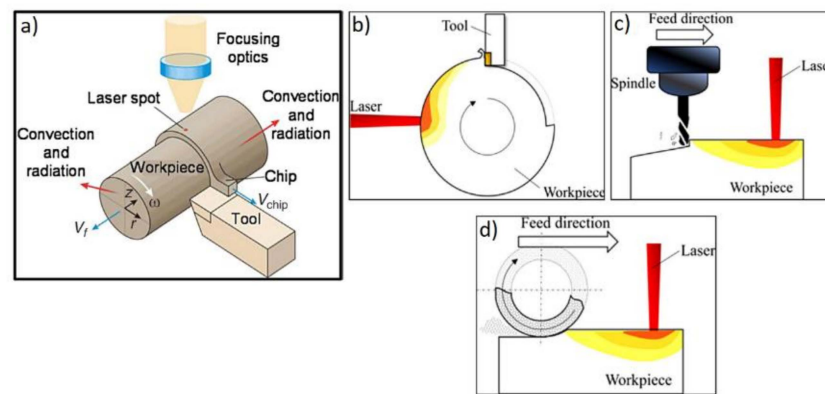


Figure 8. (a) Schematic of LAM indicating heat-losses by convection and radiation, (b) Schematic of LAM turning, (c) LAM milling, and (d) LAM grinding (adapted from [75]) (Caption: V_f —feed velocity).

3.1.1. Milling

Milling is the nomenclature given to the machining process that uses rotary cutting tools to remove excess material from the wrought stock. Nowadays, with the use of CNCs, milling can be done at a maximum of six degrees of freedom (DOF).

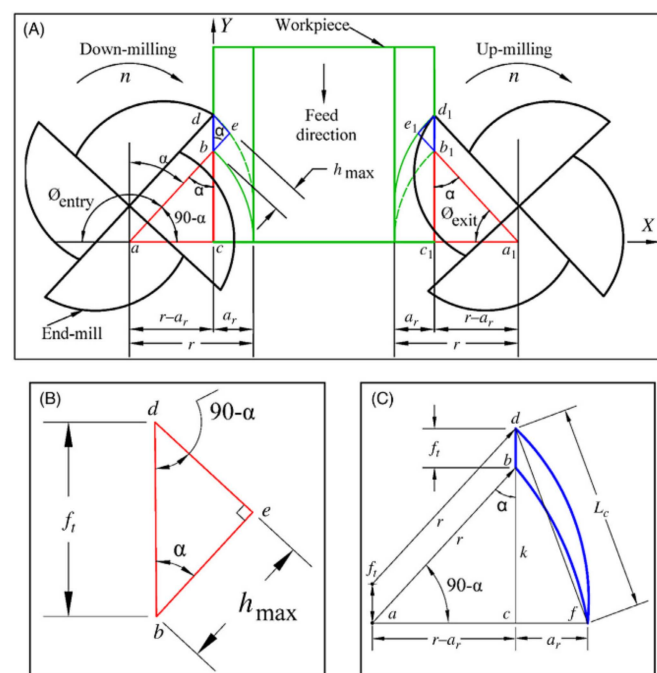


Figure 9. Chip formation showing (A) chip formation showing cutter tooth entry angle in down-milling and cutter tooth exit angle in up-milling, (B) maximum chip thickness, h_{max} , and (C) chip length, L_c [76].

Traditional milling tends to have lower a_p values and higher a_e values compared to more advanced milling techniques. However, this would cause a concentration of all heat generated in a small portion of the cutting edge, which in this case is the tip of the tool. It would require more axial passes too. This problem can be well managed in aluminium and steel alloys, but not with refractory materials like INCONEL[®] alloys. Many milling approaches can be tackled to enhance INCONEL[®] machining, such as up and down-milling, studied by Hadi et al. [77] in INCONEL[®] 718 machining, illustrated by Figure 9. Another interesting and efficient technique [78] that enriches milling INCONEL[®] 718 and 625 is trochoidal milling, illustrated by Figure 10, which consists of making the centre of the cutting tool walk a “helical horizontal” path. This procedure not only prevents tool

Author	Challenges	Remarks
Guimaraes, et al. [64]	Evaluation of how the machining processes deteriorate the surface integrity to extend the service life of the INCONEL [®] 625 components as long as possible. The influence of tool geometry, feed rate (f), and tool rotational speed (s) on surface integrity were evaluated for the milling process.	The results indicate that s has the greatest influence on specific cutting pressure (β). The parameters s and f were the main factors that affected the thickness of the cold worked zone. The results suggest that R_a after machining is driven by mechanical-thermal loadings and causes beneficial results related to corrosion resistance and compressive residual stress.
Pleta, et al. [80]	Assessment of the INCONEL [®] 718 trochoidal milling process and optimization for manufacturing scenarios. To accomplish this goal, the modelling of the cutting forces (F_c) must be investigated with semi-mechanistic methods. Furthermore, machining parameters are investigated as to how they relate to the improvement of tool life and F_c utilizing the Taguchi method.	It is found that TW increases the depth of the machining affected zone as does increasing h_{ch} . Nutational rate ($\dot{\varphi}$) and rotational rate ($\dot{\theta}$) have the largest interactions with both F_c and tool VB . It was found that h_{ch} and TW increased the depth of the plastically deformed and elongated grains in both the radial and axial orientations. The process parameters such as s, f, a_p and vegetable-based cutting fluids were optimized based on R_a and flank wear (VB). It was determined that the sound pressure and vibration signatures have a direct relation with VB . The statistical features values were extracted from the experimental data and the cutting tool VB was predicted with a mean square error (MSE) of 8.4212%. The R_a of the machined surface varies from 0.081–0.273 μm . The VB of the cutting tool varies from 0.0187–0.0254 mm. Based on the desirability function, $s = 221$ rpm, $f = 0.02$ mm/rev and $a_p = 0.17$ mm were identified as optimal process parameters. The average values of sound pressure for a brand-new, normal life (or useful life), and dull tools are 0.01955, 0.2513 and 0.4858 Pa, respectively. Similarly, the vibration signal range for a brand new, normal life (or useful life), and dull tools is 0.029–0.4394 g, 0.0780–1.32 g and 0.120–5 g.
Shankar, et al. [81]	This investigation has designed a tool condition monitoring system (TCM) while milling INCONEL [®] 625 based on sound and vibration signatures. The experiments were carried out based on response surface methodology (RSM).	

Table 6. Cont.

Author	Challenges	Remarks
Alonso, et al. [82]	Slot milling operations were performed to investigate the influence of s and machining direction in INCONEL [®] 718 alloy.	It was observed at higher s , lower values of R_a and lower torque (M) values were obtained. Moreover, the main novelty of this work is the influence of the anisotropy of Wire and Arc Additive Manufacturing (WAAM) INCONEL [®] 718 alloy on its machinability. Milling along the extruder travel direction offers better dimensional tolerance values with lower cutting M , being the more efficient way.
Boozarpoor, et al. [83]	Turn-milling technology was utilized to machine cylindrical samples of INCONEL [®] 718 alloy. The effect of process factors such as tool rotational speed (or spindle, s), workpiece rotational speed (v_c), f and eccentricity (e) on surface roughness (R_a) and tensile residual stress was analysed.	The results showed that f is the most influential parameter that determines the value of R_a and residual stress. Furthermore, by considering production rate as a constraint, it was logically discussed that a setting of 1000 rpm cutter-speed, 300 rpm work rotational speed, 0.12 mm/rev feed rate and 0.2 mm eccentricity can guarantee maximum production rate as well minimum R_a and tensile residual stress.
Anburaj and Pradeep Kumar [70]	Face milling was carried out on INCONEL [®] 625 and twenty-seven iterations (L_{27}) were conducted using Design of Experiments (DOE), including three levels of v_c and f_z with constant a_p . The study included three lubrication conditions such as dry-machining, normal coolant (wet) and cryogenic CO ₂ (l) coolant. The output responses such as cutting temperature (T_{cut}), cutting feed force (F_x), cutting normal force (F_y), cutting axial force (F_z) and R_a were evaluated.	The results were optimized using the TOPSIS technique with ANOVA tests, as the results of the highest closeness coefficient (C_i) value indicated the cryogenic CO ₂ (l) coolant environment, and the input optimized parameters were $v_c = 80$ m/min and $f_z = 0.05$ mm/tooth. Other parameters such as $T_{cut} = 57.38$ °C, $F_x = 201.5$ N, $F_y = 251.1$ N, $F_z = 335.9$ N, and $R_a = 0.159$ µm were found optimal parameters, in the 19th iteration having obtained $C_i = 0.928835$.

3.1.2. Turning

Opposed to milling, the turning process takes place in a lathe for components with a revolution axis, i.e., turbine shafts. The workpiece spins in a lathe while the fixed tools, with or without inserts, remove the surplus material. It is patent in Figure 11 the normal movement of the tool while turning a sort of shaft and some intrinsic characteristics of the inserts used. Some of the main problems in turning INCONEL[®] 718 and 625 are the specific cutting energy (SCE) and rapid augment of surface hardening upon cutting material. Moreover, since shafts must comply with certain geometric specs for the better functionality of the component, R_a is a key factor to be studied, varying v_c , f and a_p .

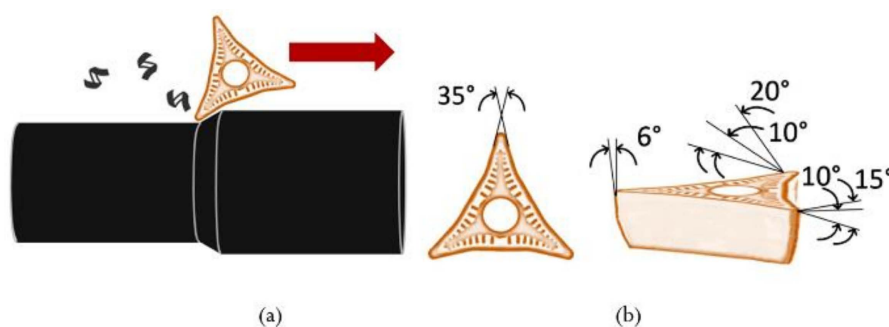


Figure 11. (a) Turning example; (b). Insert A-type (view of basic side cutting edge angle, rake angle, and secondary angles for chip breakage) [84].

Table 7 presents the latest experimental challenges and developments in the machining of INCONEL[®] with the turning process.

Table 7. Critical challenges and developments in the turning process of INCONEL®.

Author	Challenges	Remarks
Waghmode and Dabade [23]	Examination and observation of the response parameters like F_c and R_a on input parameters such as v_c , f and a_p . Experimentation was conducted as per Taguchi's L_9 orthogonal array during INCONEL® 625 alloy turning operation. The results are analysed using the ANOVA method.	ANOVA suggests that the a_p has a 55.05% contribution to F_c . In thrust force (F_z), the contribution of a_p is 55.83% which is the parameter with the most influence. As a_p increases, F_z increase. The main contribution for the feed force is provided by the a_p , with 83.39%. Parameters f and a_p highly affect R_a , having 20.61 and 51.68% contribution, respectively. As f increases, R_a increases too. With parameter v_c , it shows an inverse trend.
Kosaraju, et al. [25]	A multi-objective optimization based on the Taguchi-based Grey Relation Analysis (TGRA) method was employed to find the optimal levels of turning INCONEL® 625 parameters for the objective of lower F_c and better R_a under dry-cutting conditions.	From the statistical analysis, the results show that f is identified as the most significant parameter for the turning operation according to the weighted sum of F_c and R_a . The optimal combination of control factors and their levels are $v_c = 75$ m/min, $f = 0.103$ mm/rev and $a_p = 0.2$ mm.
Vignesh and Ramanujam [75]	Evaluate the influence of laser-assisted high-speed machining (LAHSM) on the F_c (F_z in Figure 8), R_a , TW and the chip morphology during the INCONEL® 718 turning process.	LAHSM optimal parameters were $v_c = 80$ m/min, $f = 0.08$ mm/rev and laser power, $P_{\text{Laser}} = 1300$ W. F_c , R_a and TW values were better over the conventional turning process ones, leading to a reduction of F_c by 24.5%, R_a by 56% and TW by 29%.
Raykar, et al. [85]	High-pressure cooling (HPC) of cutting tools can be very effective when machining difficult-to-cut materials like INCONEL® 718. An analysis of microhardness and degree of work hardening (DWH) is carried out to evaluate the machinability of the INCONEL® 718 alloy while turning in a high-pressure coolant environment.	Microhardness has a sudden change between 30–120 μm below the machined surface. After this region, the microhardness value is similar to the bulk, which is found at 270–300 μm below the machined surface for all samples. The microhardness near the machined surface is found to be $1.11 \times$ the bulk microhardness. Microhardness variation is unaffected by the changes in the process parameters since none is statistically significant at a 95% confidence level. A significant microhardness value is noticed at a depth of 90 μm .
Infante-García, et al. [86]	The increase of the undeformed chip cross-section and the high SCE of INCONEL® 718 give rise to load peaks during machining. Different tests involving multipass finishing turning have been carried out to study the magnitude of the load peaks for different cutting conditions.	Initial results have shown a significant peak in the machining loads, predicted by Altintas force law [87]. This peak is related to the tool tip radius and the cutting parameters, after the second and successive passes. The main factor that contributes to that is the increase of undeformed chip cross section during a short interval. Thus, the progression of TW is significantly influenced. The machining load at the end of a turning pass can significantly increase during a short interval. Consequently, this effect may influence TW progression leading to premature tool failure.
Makhesana, et al. [88]	The turning tests to INCONEL® 625 are conducted under dry, MQL, and nanofluid-MQL (nMQL) environments and the machining results are compared considering R_a , chip morphology, TW, T_{cut} , P_{in} and microhardness	Sunflower oil blended with MoS_2 resulted in 56, 42, and 22% improved R_a compared to dry, MQL, and nMQL (Graphite) conditions, respectively. Also, the efficiency of nMQL with graphite and MoS_2 is evaluated by slower TW progression. Also, MQL, nMQL with MoS_2 , and nMQL (graphite) resulted in lower T_{cut} by 18, 35, and 25%, respectively, compared to dry turning. The effective performance of nMQL is credited to the better penetration ability of the applied lubricant. Furthermore, the MQL application with compressed air facilitated chip removal and heat dissipation during machining.

Table 7. Cont.

Author	Challenges	Remarks
Airao, et al. [89]	Examination of the machinability of the INCONEL [®] 718 alloy in conventional and ultrasonic assisted turning (UAT) under dry, wet, minimal quantity lubrication (MQL), and CO ₂ (l) strategies. The experiments are performed in an in-house developed ultrasonic-assisted turning (UAT) setup, keeping all the machining parameters constant.	The CO ₂ (l) reduces edge chipping, nose wear, adhesion, and abrasion wear. The conventional turning under CO ₂ (l) reduces the VB by 32–60% and power consumption (P_{in}) by 5–31% compared to dry, wet, and MQL strategies. Similarly, the UAT under CO ₂ (l) reduces the VB by 32–53% and P_{in} by 11–40% compared to dry, wet, and MQL strategies. The UAT reduces R_a compared to conventional turning when used under MQL and CO ₂ (l). The CO ₂ (l), in conjunction with ultrasonic vibration, significantly reduces SCE and TW without compromising R_a . Moreover, this combination also helps in enhancing the chip breakability and reducing ϵ concentration.

3.1.3. Drilling

Drilling is a cutting process where a drill bit is spun to cut a circular hole in a component. In INCONEL[®] applications, drilling is important to create micro holes that will permit the cooling of gas turbines, as illustrated by Figure 12 and studied by Venkatesan et al. [90] on the hole quality assessment in INCONEL[®] 625 alloy parts.

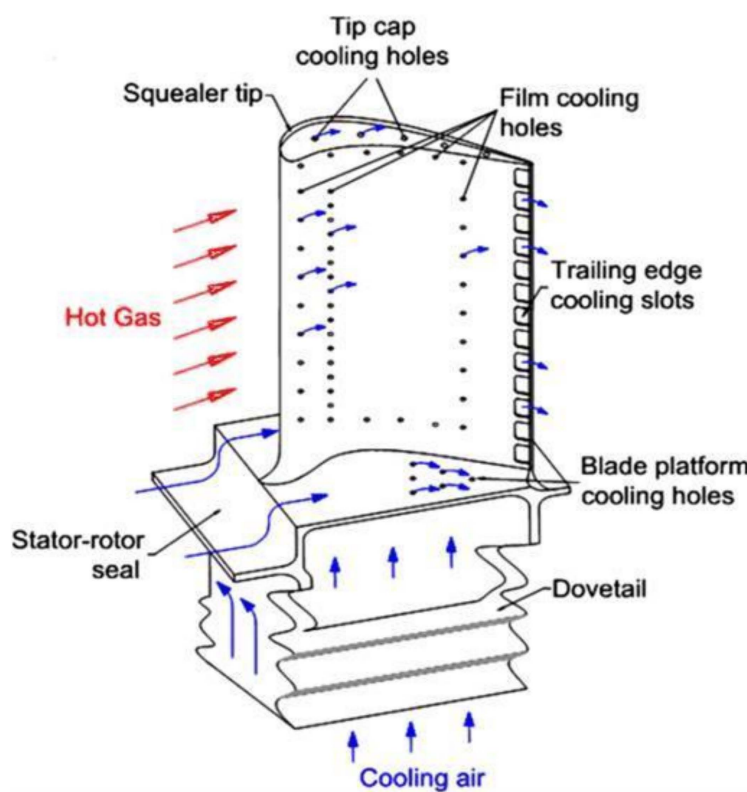


Figure 12. Gas turbine blade cooling schematic [91].

The INCONEL[®] 718 alloy has many challenges in deep-hole-drilling as well since the process is prone to drill jamming due to material expansion inside the holes. Table 8 presents the latest experimental challenges and developments in the machining of INCONEL[®] alloys with the drilling process.

Table 8. Critical challenges and developments in the drilling process of INCONEL®.

Author	Challenges	Remarks
Neo, et al. [92]	The traditional carbide-tipped gun drills often get worn at an accelerated rate and require repetitive re-sharpening or replacement when drilling INCONEL® 718 alloys. This occurrence lowers productivity and increases costs. Furthermore, it is also a challenging task to meet the stringent hole-straightness requirement of 1/1000 mm for deep-hole drilling (DHD).	In contrast to traditional carbide-tipped gun drills, the developed PCBN-tipped gun drill can operate at higher v_c and reduce drilling forces, drilling M , and TW . Furthermore, the surface quality of drilled holes is much better than those drilled by traditional carbide gun drills. For a stable drilling condition, it is also recommended to perform deep-hole drilling with the developed PcBN gun drill on INCONEL® 718 at $v_c \geq 50$ m/min.
Venkatesan, et al. [90]	Drilling micro-cooling holes in turbine blades on INCONEL® 625 is one of the noteworthy applications of micro-drilling, and few are the investigations on the hole quality assessment and drill bit tool life. The multi-response optimization of test parameters in micro-drilling conditions is presented, using the approach on the Taguchi L_{27} design. Micro-drilling is performed in a 2 mm plate thickness of INCONEL® 625 with an uncoated micro-drill.	After each drilling test, the hole diameter, circularity error, overcut, taper ratio, cylindricity and hole damage factor are measured, and the results are examined. The deviation in hole diameter, cylindricity, circularity error, roundness, overcut, taper ratio, and hole damage factor obtained is increased to 5.5, 87.2, 50.5, 5.7, 77.4, 20.0 and 5.4%, respectively, from 1st to 25th hole. Better hole quality features with the least deformed layer thickness and low burr formation at entry, and exit, are consistently achieved with $s = 21,000$ rpm and $f = 6$ mm/min for a given tool diameter. The optimized parameters are a tool diameter of 0.8 mm, (the most suitable tool diameter for hole quality and productivity in micro-drilling), $s = 21,000$ rpm and $f = 10$ mm/min. Chip clogging, entrance burr, and exit burr are obtained before the tool failure. These new findings have brought out a highly beneficial database for aerospace industries without losing the quality of the hole in production.
Sahoo, et al. [93]	Use of cryogenically treated drill bits in INCONEL® 718 alloy machining. Drill bits are conditioned under two different environments i.e., cryogenically treated with single-tempered drill bits, and cryogenically treated with double-tempered drill bits. The Taguchi method was used for trial design and optimization of factors along with the Whale optimization algorithm.	Results show that f is the most contributing parameter to maximize F_z , while s is the most contributing parameter to maximising M . Also, tool condition is the most contributing factor to minimising R_a . By maximizing the F_z , up to 184 N, and M , up to 0.72 Nm, during drilling operation on INCONEL® 718, using cryogenically treated and single tempered drill bit, it was found that the optimal parameter settings were $s = 215$ rpm and $f = 0.106$ mm/rev. R_a was minimized to 3.77 μ m. It was also seen that cryogenically treated and the single-tempered drill bit was more influential in attaining maximum F_z and M , while cryogenically treated and the double-tempered drill bit was more influential in attaining minimum R_a .

3.1.4. Boring

Boring is the manufacturing process in which previously drilled holes are enlarged by a single-point cutting tool. Not much information is available about the boring process on INCONEL® alloys whereby it is only presented in the study carried out by Ratnam et al. [94], whose challenges involved the investigation of the machining parameters' effect on R_a , TW , F_c on the cutting tool and workpiece vibration during dry boring of INCONEL® 718 with TiCN-Al₂O₃-TiN coated inserts using response surface methodology (RSM). It was found that the use of accelerometers, radioactive sensors and piezoelectric actuators does not make it possible to measure rotating objects' vibrations. On the other hand, the LDVs are capable to measure rotating objects' vibrations with a simple experimental arrangement. Parameters s and f were found to have a significant influence on R_a . The parameter

a_p was found to be significant on VB , F_c , and workpiece vibration amplitude (VA). The optimal machining parametric combination was obtained using the desirability function. Cutting condition parameters such as $s = 360$ rpm, $f = 0.14$ mm/rev and $a_p = 0.4949$ mm was obtained for $VA = 38.7$ μ m, minimum $F = 117.8$ N, $VB = 0.3$ mm and minimum $R_a = 2.55$ μ m. The proposed RSM approach was an easy method to obtain maximum information with a smaller number of experiments. and successfully used by different authors in the improvement of process parameters.

3.2. Non-Conventional Manufacturing Processes—Electrical Discharge Machining (EDM)

This review also presents some new insights into a non-conventional process, which is Electrical Discharge Machining (EDM). The process is a non-conventional machining method that allows the production of pieces with complex shapes, and it can be used in materials such as INCONEL[®] 718 and 625. This particular manufacturing technique removes material from the wrought-stock thanks to melting and vaporising cavities using electrical discharges that come from a scrolling wire [95], as illustrated in Figure 13.

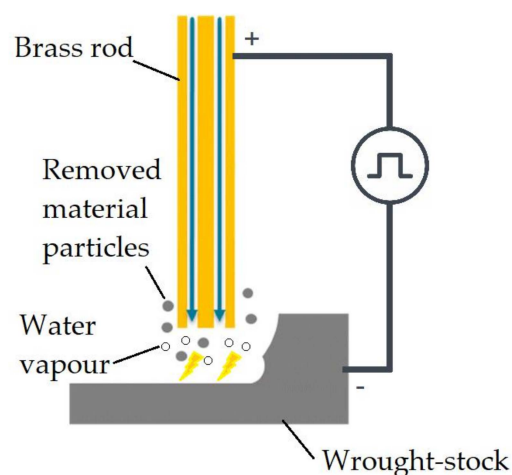


Figure 13. Schematic representation of the EDM experiment setup (adapted from [96]).

Table 9 presents the latest experimental challenges and developments in the machining of INCONEL[®] alloys with EDM.

Table 9. Critical challenges and developments in the EDM process of INCONEL[®].

Author	Challenges	Remarks
Mohapatra, et al. [39]	Comparative study of the chemical and mechanical properties of INCONEL [®] 718, 625, 825 and 601. Evaluation of the machinability of different grades of alloys using EDM.	An increase in the peak current resulted in improved material removal rate (MRR) by keeping the gap voltage (V_g), pulse-on time (T_{on}), duty factor (τ) and dielectric circulation flushing pressure (F_p) fixed at a constant value, for the different INCONEL [®] grades. An increase in R_a is observed by incrementing the peak discharge current (I_p). In the case of surface crack density (SCD), with an increase in I_p , SCD ends to decrease, again followed by an increasing trend; and then finally remained constant.
Manikandan, et al. [97]	INCONEL [®] 625 is one of the hard-to-machine materials extensively used in high-temperature applications. It has better strength and lower k , compared with more common materials, which leads to poor machinability by traditional processes. To overcome such kind of disadvantages, unconventional manufacturing methods have been developed and proposed to be suitable substitutes, such as WEDM.	This work details a single-aspect optimization problem of WEDM of INCONEL [®] 625 with the help of Taguchi analysis. In this investigation, the MRR and Overcut (OC) were deemed as the performance characteristics, and the Taguchi response showed that the best parameter combination to maximize the performance of R_a is $T_{on} = 30$ μ s, $T_{off} = 15$ μ s and $I_p = 3$ A. The best set of process parameters for attaining better OC is $T_{on} = 30$ μ s, $T_{off} = 5$ μ s and $I_p = 1$ A. Contour plots were also explored to reveal the combined influence of process parameters on the preferred performance measures.

Table 9. Cont.

Author	Challenges	Remarks
Hussain, et al. [98]	Cost reduction in machining through increased MRR using optimum machining process parameters. An experimental study is presented for optimizing process parameters T_{on} , I_p and T_{off} to maximize MRR for subtracting material from INCONEL [®] 625 work part using Taguchi DOE and its analysis.	A Taguchi orthogonal array L_9 is applied for experimental design and analysis. Optimized values of performance factors obtained by analysis are $I_p = 12$ A, $T_{on} = 160$ μ s, and $T_{off} = 35$ μ s. The maximum MRR, of 24.48 mm ³ /mm, was obtained with optimum values of performance parameters. Under these conditions, it was found that, $R^2 = 98\%$ which reflects a high confidence level in the experiment. It is also found that both T_{off} and I_p have a considerable impact on MRR. This is because higher values of T_{on} and I_p enhance the amount of energy discharge on the workpiece, which leads to increased material melting and vaporisation. MRR, kerf width (K_w), and R_a were considered as the quality measures. In the WEDM process, the brass wire electrode worked as expected and the optimal arrangement of input factors was found as $T_{on} = 140$ μ s, $T_{off} = 50$ μ s, $SV = 60$ V, and $WT = 5$ kg, which are the most relevant factors with a $C_i = 0.989$. The MRR efficiency was found to vary from: 1.3389–29.3128 mm ³ /min for INCONEL [®] 625; 1.1844–31.5995 mm ³ /min for INCONEL [®] 718. R_a was found to vary from: 4.7–11.5333 μ m for INCONEL [®] 625; 6–12.3667 μ m for INCONEL [®] 718. Optimal parameters setting determined as: [$V_g = 80$ V, $I_p = 7$ A, $T_{on} = 200$ μ s, $\tau = 75\%$, $F_p = 0.6$ bar] for INCONEL [®] 625 [$V_g = 70$ V, $I_p = 7$ A, $T_{on} = 500$ μ s, $\tau = 80\%$, $F_p = 0.6$ bar] for INCONEL [®] 718.
Liu, et al. [95]	Enhancing the machining process of INCONEL [®] 718 using zinc-diffused coating brass wire electrode and Taguchi-Data Envelopment Analysis-based Ranking (DEAR).	A significant carbon enrichment due to the thermo-mechanical effect of EDM was noticed on the machined surface of INCONEL [®] 718 and 625, during EDM operation, attributed to the formation of carbides and grain refinement, which increased micro-strain as well as dislocation density. The increase in I_p resulted in improved MRR (while keeping V_g , T_{on} , τ and F_p constant) for different INCONEL [®] alloys. R_a was observed to increase as I_p increased. Process parameters are more influential on radius deviation as compared to angular error. At $F_p = 4$ kg/cm ² , the radius deviation is around 4%, which increased to 5.4% at $F_p = 12$ kg/cm ² . A low F_p value agglomerates debris, which resulted in a coarser surface due to the re-solidification, with a $R_a = 2.12$ μ m. However, with the increase of F_p to 12 kg/cm ² , the surface quality improved and resulted in $R_a = 1.93$ μ m. An increasing trend is observed where S_G increased with the magnitude of F_p . Using $F_p = 4$ kg/cm ² resulted in $S_G = 107$ μ m. With the increase up to $F_p = 12$ kg/cm ² , values of $S_G = 111.5$ μ m were attained. Similarly, an increase in ϕ_N from 4 mm to 8 mm not only increased S_G from 108.5 μ m to 110 μ m but also increased angular error from 0.255% to 0.6%. The high ϕ_N increased the entry of dielectric flow, which hindered the stability of the thermo-electric erosion process near corners. The F_p and ϕ_N parameters showed a significant effect on the R_a . The optimized parametric settings are $SV = 50$ V, $F_p = 4$ kg/cm ² , $\phi_N = 8$ mm, and $W_D = 10$ mm. The confirmatory experiment reduced the process's limitations to an $S_G = 109$ μ m spark gap, 0.956% angular error, 3.49% cylindricity error, and $R_a = 2.2$ μ m.
Rahul, et al. [99]	INCONEL [®] 718, 625, 825 and 601 machinability was experimentally analysed during the execution of EDM. The experimental design was planned according to a 5-factor/4-level L_{16} orthogonal array. The following process variables were considered: V_g , I_p , pulse-on time (T_{on}), duty factor (τ) and F_p . Machinability was assessed in consideration of MRR, electrode wear rate, R_a and surface crack density (SCD) at the already worked surface. The satisfaction function approach integrated with the Taguchi method was attempted to determine optimal parameter settings.	
Farooq, et al. [100]	Several developments in WEDM have been reported, but the influence of F_p attributes has not been thoroughly investigated. The influence of four process variables, namely servo voltage, F_p , nozzle diameter (ϕ_N), and nozzle-workpiece distance (W_D), were analysed on INCONEL [®] 718 concerning geometrical errors (angular and radial deviations), spark gap (S_G) formation, and R_a . In this regard, detailed statistical and microscopical analyses are employed with mono and multi-objective process optimization by employing the TGRA method.	

3.3. Tool Wear

With the tool operation in machining, wear starts to be a key factor in quality and productivity, namely with INCONEL[®] alloys, such as 718 and 625. To identify a worn milling tool, the ISO 8688-2 [101] standard predicts that a tool presenting either $VB = 300 \mu\text{m}$ or $VB_{\text{max}} = 500 \mu\text{m}$ on the flank is considered a worn tool [69]. For turning tools or inserts, the ISO 3685 standard is the one to consult [102]. Taking into account a novel lubrication method, Bartolomeis et al. [69] observed that the tool wear behaviour mechanisms during EL conditions were abrasion and microchipping on the cutting edge, due to the tendency of INCONEL[®] 718 to develop BUE.

Figure 14 packs the initial causes of wear, the various wear mechanisms that lead to different types of wear and the final consequences from the tool-wear due to INCONEL[®] machining. As a complement to Figure 14, Table 10 presents the typical TW mathematical models, used to characterize the numerous TW mechanisms. It is suggested to consult the work of Wang et al. [37] to better understand the additional variables described in Table 10.

Table 10. Typical TW mathematical models (adapted from [37]).

Authors	TW Model	Comments
Taylor [103]	$C = v_c \cdot T_{\text{tool}}^n$ or $T_{\text{tool}} = \frac{C}{v_c^{1/n} \cdot f^q \cdot a_p^p}$	Taylor's empirical tool life model.
Archard [104]	$V = k \cdot \frac{P \cdot L}{3 \cdot \sigma_s} = k \cdot \frac{P \cdot L}{H}$	Abrasive wear model.
Usui [105,106]	$\frac{dw}{dt} = A_1 \cdot \sigma_n \cdot v_s \cdot e^{-\frac{B_1}{T}}$	Diffusive wear model.
Takeyama [107]	$\frac{dw}{dt} = G(v, f) + D \cdot e^{-\frac{Q}{RT}}$	Abrasive and adhesive wear model.
Childs [108]	$\frac{dw}{dt} = \frac{A}{H} \cdot \sigma_n \cdot v_s$	Abrasive and adhesive wear model.
Schmidt [109]	$\frac{dw}{dt} = B \cdot e^{-\frac{Q}{RT}}$	Diffusive wear model.
Luo [110]	$\frac{dw}{dt} = \frac{A}{H} \cdot \frac{F_n}{v_c \cdot f} \cdot v_s + B \cdot e^{-\frac{Q}{RT}}$	Abrasive, adhesive, and diffusive wear model.
Astakov [111,112]	$hs = \frac{dh_r}{ds} = \frac{100 \cdot (h_r - h_{r-i})}{(1 - l_i) \cdot f}$	Surface wear model.
Attanasio [113,114]	$\begin{cases} \frac{dw}{dt} = D(T) \cdot e^{-\frac{Q}{RT}} \\ D(T) = D_1 \cdot T^3 + D_2 \cdot T^2 + D_3 \cdot T + D_4 \end{cases}$	Diffusive wear model, presenting the T -dependent diffusive coefficient.
Pálmai [115]	$\frac{dW}{dt} = \frac{v_c}{W} \cdot \left[A_\alpha + A_{th} \cdot e^{-\frac{B}{v_c^x + K \cdot W}} \right]$	TW model, considering the effects of wear-induced cutting, force, and T rise on TW.
Halila [116,117]	$W = N \cdot \sum_{i \geq i \min j=1}^I P_r^R(R_i) \cdot P_r^\phi(\phi_j) \cdot \frac{R_i^2 \cdot P}{2 \cdot H_i \cdot \tan(\phi_j)} \cdot v_c$	TW model is dependent on the material removal rate.

3.4. Tool Materials

As previously mentioned, due to poor k from INCONEL[®] alloys, which lead to a substantial increase of T in the three heat-zones when machining, the used tools are more prone to premature wear since the heat generated will end up creating BUE, which will rapidly degrade coatings and the tool material itself. The TW mechanisms, which include abrasive wear, adhesive wear, and plastic deformation, are following described. Severe TW is one of the key reasons for machining inefficiency [118].

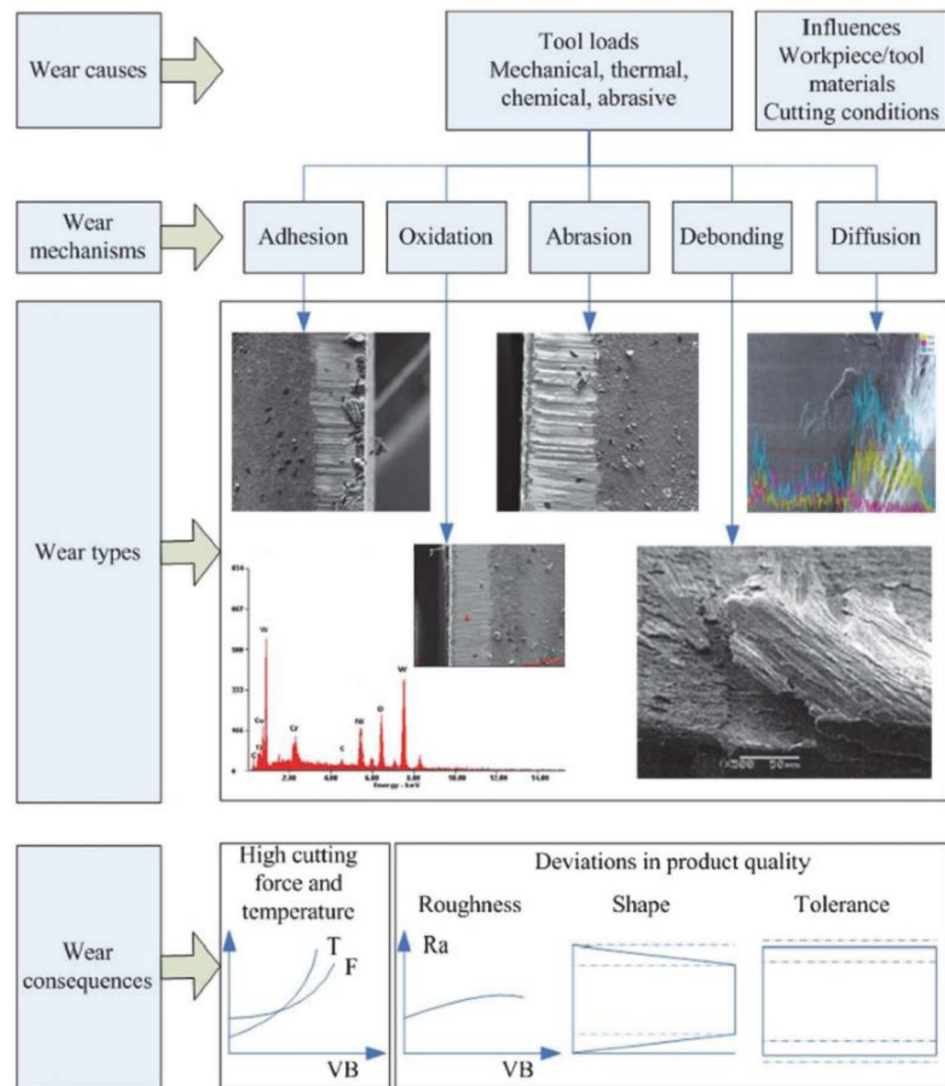


Figure 14. The wear causes, wear mechanisms, wear types, and wear consequences in the cutting of Ni-based superalloys [118].

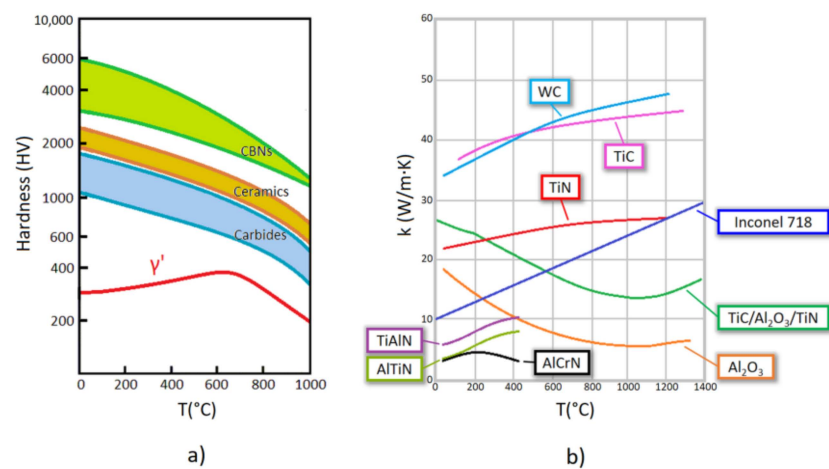


Figure 15. (a) Hot hardness characteristic curve of CBN, Ceramic and Carbide tool materials compared with the γ' structure of INCONEL[®] 718, (b) Thermal conductivity of tungsten carbide (WC), INCONEL[®] 718 and different coatings for carbide tools against T (adapted from [119]).

Tool materials, depending on their application, may vary as hard metal, high-speed steel (HSS, and its variant HSS-Co), cermets, ceramics (where carbides are inserted), PcBN and many more. Table 11 presents the latest experimental observations and performance of non-coated tools in the machining of INCONEL[®] alloys.

Table 11. Machinability performance during non-coated tools assisted machining of INCONEL[®].

Author	Machining Type Material	Tool Material and Cutting Conditions	Remarks
Infante-García, et al. [86]	Turning INCONEL [®] 718	PcBN inserts $v_c = 300$ m/min $f = 0.07, 0.1$ and 0.15 mm/rev $a_p = 0.15, 0.25$ and 0.5 mm	A significant peak in the machining forces, predicted by the Altintas force law [87], is related to the tool tip radius and the cutting parameters, after the second and successive passes. The rapid development and magnitude of the peak loads influence the tool wear progression, as a premature notch developed along the cutting edge, observed after the test with $a_p = 0.5$ mm and $f = 0.15$ mm/rev. The low machinability of INCONEL [®] 718, along with the brittleness of PCBN tools, leads to a premature failure of the cutting tool when this phenomenon is not considered in conventional turning. The ISO 3685:1993 [102] standard was used as a reference for the VB measurement. Pulsed laser ablation (PLA) using ns-laser leads to a transformation of cBN to hBN in all considered laser parameter combinations. The cutting tool hardness is significantly decreased by the hBN formation, from over 3400 HV down to 1700 HV. However, not all laser parameters reduce hardness by the same amount. Tools with laser-prepared cutting edges achieve comparable tool wear to reference tools when applying appropriate laser parameters. There is an indication that the transformed hBN acts as a solid lubricant, which leads to a decrease in the cutting forces.
Breidenstein, et al. [120]	Turning INCONEL [®] 718	PcBN inserts. $V_c = 200$ m/min $f = 0.1$ mm/rev $a_p = 0.2$ mm	
Rakesh and Chakradhar [121]	Turning INCONEL [®] 625	Uncoated inserts ISO ref: CNMP120408	The ISO 3685:1993 [102] standard was used as a reference for the VB measurement. Among all four cooling conditions, the minimum R_a , VB , and main F_c were obtained for cryogenic machining using N ₂ (l)-air mixture as a coolant. This result indicates that cryogenic coolants are well-suitable for the machining of INCONEL [®] 625 alloys. The lowest $R_a = 0.481$ µm was obtained under cryogenic machining with the parameter setting of $v_c = 60$ m/min, $f = 0.15$ mm/rev, and $a_p = 0.6$ mm. Reductions of 38.49%, 34.56% and 30.08% in R_a were achieved with cryogenic machining when compared to dry, MQL and nMQL, respectively, under the same parameters. The minimum value of VB was observed at the lowest levels of cutting parameters, irrespective of the cooling conditions. Also, the lowest $VB = 85.52$ µm was noticed under cryogenic machining, when machining with parameter settings of $v_c = 60$ m/min, $f = 0.05$ mm/rev and $a_p = 0.6$ mm. The VB reductions by cryogenic machining, when compared to dry, MQL and nMQL, are 20.32%, 11.42%, and 8.81%, respectively.
		Level 1 $v_c = 40$ m/min $f = 0.05$ mm/rev $a_p = 0.2$ mm Dry machining	
		Level 2 $v_c = 50$ m/min $f = 0.1$ mm/rev $a_p = 0.4$ mm MQL	
		Level 3 $v_c = 60$ m/min $f = 0.16$ mm/rev $a_p = 0.6$ mm nMQL	
		Level 4 $v_c = 70$ m/min $f = 0.2$ mm/rev $a_p = 0.8$ mm Cryo N ₂ (l)	
		Level 5 $v_c = 80$ m/min $f = 0.25$ mm/rev $a_p = 1$ mm	

Table 11. Cont.

Author	Machining Type Material	Tool Material and Cutting Conditions	Remarks
Zhang, et al. [103]	Turning INCONEL® 718	WC insert $v_c = 80, 160$ and 240 m/min $f = 0.005, 0.01$ and 0.015 mm/rev $a_p = 0.15, 0.2$ and 0.25 mm	A high-speed ultrasonic vibration cutting (HUV) method has been proposed for the precision machining of INCONEL® 718. The TGRA L ₉ array method was used for analysis. Owing to the limitations of the cooling pressure and duty cycle, the useful highspeed stable region for INCONEL® 718 was $v_c = 80\text{--}300$ m/min. In this range, compared to the conventional effective cutting region, the cutting efficiency was significantly improved. The HUV-Taylor's equation developed in this study aimed to provide a comprehensive understanding of the most recently proposed high-speed ultrasonic precision machining methods and provided guidance for appropriate practical applications in the future. The impact effect due to the tool-workpiece separation was a factor that needs to be suppressed. This effect was the core reason for the failed region in ultra-high-speed machining. In this regard, developing the impact-resistant tool could be seen as the next meaningful work for further cutting speed enhancement. VB was measured according to the instructions of the ISO 3685:1999 standard [102] It was characterized using white-light interferometry (WLI), scanning electron microscopy (SEM), and electron backscatter diffraction (EBSD). Wear topography and surface-induced plastic deformation were evaluated. Abrasion marks and grooves on different length scales indicate that VB was caused by abrasion during sliding contact of the tool with the workpiece. Examination of worn WC grains employing EBSD proved to be a suitable method to assess the contribution of plastic deformation to TW in metal cutting. This method is of particular interest to developing a deeper understanding of relative wear rates associated with the machining of different workpiece classes and alloys. The parameter $VB = 185\text{ }\mu\text{m}$ is below the maximum limit imposed by the standard.
Hoier, et al. [122]	Turning INCONEL® 718	WC-Co $v_c = 30$ m/min $f = 0.075$ mm/rev $a_p = 1$ mm $t = 16.2$ min	

3.5. Tool Coatings

Some tool materials have enough hardness to cut through INCONEL®, as it is shown in Figure 15, although others require a coating to protect the core material from abrasion when machining. The binomial substrate/coating is selected, as a function of specific requisites, from each application which often demands from the cutting tool antagonistic characteristics like tenacity and hardness. The usage of coated tools is highly advantageous from a production point of view, not because it is only possible to escalate v_c or s values, but also to promote better quality to the fabricated components, and some of them can be multilayer, in which each layer has its unique function. The preferred manufacturing processes to make coated tools are metallurgical powder processes, chemical vapour deposition (CVD) or even physical vapour deposition (PVD).

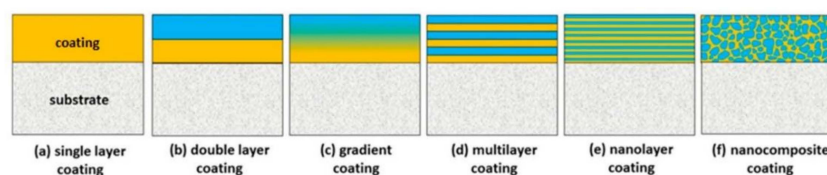


Figure 16. Scheme of how different types of coatings look when applied on the substrate [123].

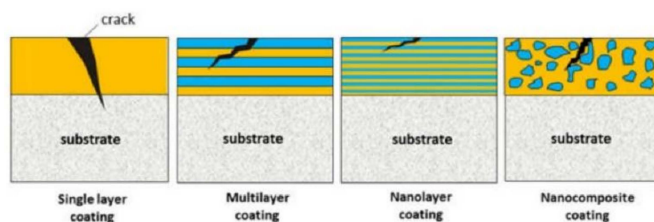


Figure 17. Crack propagation behaviour for each of the common coating structures [124].

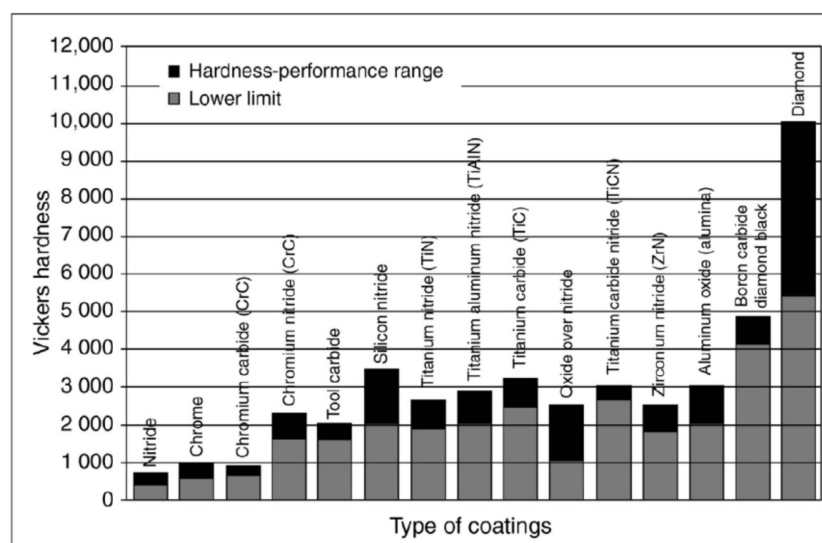


Figure 18. The hardness of different coating materials with a lower limit and suitable performance range [125].

A schematic of how different coatings can appear in a tool is presented in Figure 16, whereas Figure 17 demonstrates how crack propagation occurs inside the coatings due to TW. Figure 18 shows the lower limits and the hardness performance range of some of the most used tool coatings. Examples of preferred coatings to machine INCONEL[®] 718 include TiAlN, TiAlCrN, TiCN, TiN/AlTiN, and TiAlCrSiYN/TiAlCrN [126].

Table 12 presents the latest experimental observations and performance of coated tools in the machining of INCONEL[®].

Table 12. Machinability performance during coated tools assisted machining of INCONEL[®].

Author	Machining Type Material	Tool Coatings and Cutting Conditions	Remarks
Zhao, et al. [53]	Turning INCONEL [®] 718	TiAlN coated carbide tool. WC uncoated tool $v_c = 40, 80$ and 120 m/min $f = 0.1$ mm/rev	Irrespectively of the tool type, the tool-chip contact length was decreased with the increase of v_c . The tool-chip contact length and crater wear for the PVD AlTiN coated carbide tool was decreased compared with that of the uncoated carbide tool in dry orthogonal cutting of INCONEL [®] 718. A PVD AlTiN coated carbide tool decreased by $5.94 \mu\text{m}$ or 5.26% the h_{ch} , compared with an uncoated tool at $v_c = 120$ m/min. The maximum T_{cut} for the PVD AlTiN coated carbide tool decreased by 14.00°C or 2.11% , 25.00°C or 3.64% , and 39.00°C or 5.47% , compared with that for an uncoated WC tool in dry orthogonal cutting of INCONEL [®] 718 at $v_c = 40, 80$ and 120 m/min, respectively. For uncoated carbide tools, the relative error ($\Sigma \delta $) from the predictive model- R_{G-W} , compared to the measured T at $v_c = 40, 80$ and 120 m/min was 31.83% . $\Sigma \delta $ from other predictive models were 56.16% (model- R_{L-SH}), 53.54% (model- R_{SH}), 96.06% (model- R_{K-F}), 157.62% (model- R_{L-SU}), 119.32% (model- R_{G-W}), 41.52% (model- R_R) and 96.87% (model- R_{T-K}). For PVD AlTiN coated carbide tools, $\Sigma \delta $ from the predictive model- R_R , compared with the measured T at $v_c = 40, 80$ and 120 m/min was 52.61% . $\Sigma \delta $ from other predictive models were 147.44% (model- R_{L-SH}), 159.99% (model- R_{SH}), 76.48% (model- R_{K-F}), 63.00% (model- R_{L-SU}), 128.72% (model- R_{G-W}), 136.25% (model- R_{B-K}) and 76.22% (model- R_{T-K}).

Table 12. Cont.

Author	Machining Type Material	Tool Coatings and Cutting Conditions	Remarks
Montazeri, et al. [126]	Turning INCONEL® 718	Uncoated carbide tool, TiAlN-coated carbide tool, Al-Si coated carbide tool. $v_c = 50$ m/min $f = 0.1$ mm/rev $a_p = 0.15$ mm	Results showed that the proposed soft Al-Si coating can provide a solution to the outlined machining challenges of INCONEL® 718. The tool life of the Al-Si coating was more than $6\times$ higher than that of the uncoated tool and around $3\times$ higher than the TiAlN coating, and the F_c of the soft Al-Si coating was around $1/2$ that of the uncoated tool. These improvements can be attributed to better lubricity and frictional behaviour in the tool-chip interface due to the superior lubricity of the Al-Si coating, which resulted in lower adhesion and BUE formation, less contact pressure at the cutting zone and lower friction.
Agarwal, et al. [127]	Milling INCONEL® 718	TiAlN-coated carbide insert $s = 501, 902$ and 1203 rpm $f = 0.25$ mm/tooth $a_p = 1$ mm Emulsion Flood-Cooling (EFC)	The proposed method was implemented in the form of an automated computational program, and a series of experiments were performed to analyse the progression of the VB area of the tool over the volume of material removed. Based on the outcomes of the present study, it has been realized that the image processing method presented in this study can accurately and efficiently evaluate the VB width and wear area. Also, the proposed methodology was able to replicate the well-known curve of the VB area versus the volume of material removed.
Liu, et al. [128]	Turning INCONEL® 625	PVD-TiAlN coated carbide tools $v_c = 25\text{--}175$ m/min $f = 0.02\text{--}0.3$ mm/rev $a_p = 0.5$ mm expected $t \geq 10$ min	The turning experiment of INCONEL® 625 with a PVD-TiAlN-coated carbide tool exceeded $t = 10$ min. It was found that the main TW morphologies of the tool were the BUE, crater wear, chipping, tipping, and fracturing. The main TW mechanisms were abrasion, adhesion, and oxidation. Adhesion wear under low v_c yielded a BUE wear morphology, whereas adhesion wear and oxidation wear under high v_c resulted in crater wear. As v_c and f further increased, the tool began to peel, tip, or even fracture. A two-dimensional TW map based on v_c and f was drawn. In the wear map, three tool failure limits, i.e., BUE limit; crater wear limit; and chipping, tipping, and fracture limit were determined. A safety zone was planned to determine the optimum cutting parameter range. A method of optimizing the cutting parameters by combining the wear map, tool wear, and R_a of the machined workpiece was proposed. The optimum cutting parameters were $v_c = 60$ m/min, $f = 0.1$ mm/rev, and $a_p = 0.5$ mm. A complete tool life experiment was performed with the optimized cutting parameters and a tool life distribution model obeying a normal distribution was established. When reliability was 0.9, the recommended tool-life was 70 min.
Criado, et al. [129]	Turning INCONEL® 718	TiAlN + TiN coated carbide insert. $v_c = 250\text{--}300$ m/min $f = 0.1\text{--}0.15$ mm/rev $a_p = 0.15$ mm TiN-coated PcBN insert $v_c = 50\text{--}70$ m/min $f = 0.1\text{--}0.15$ mm/rev $a_p = 0.25$ mm PVD TiAlN ₂ coated carbide inserts.	Carbide tools have a longer tool life than PcBN tools, but PcBN tools higher allow speeds between $4x$ and $6x$. In terms of machined surface per edge, it has been proven that, at $f = 0.15$ mm/ver, more machined volume is obtained, while for $f = 0.1$ mm/rev, the machined surface quality is maintained in the PcBN tools. For this reason, the viability of using PcBN tools in finishing operations in INCONEL® 718 is demonstrated. The best combination found for the PcBN tool was at $v_c = 250$ m/min and $f = 0.15$ mm/rev. It was found that the tool life increases at low cutting speeds, although f does not affect it significantly. The finished surface machined with the PcBN tool obtains a more constant behaviour and excellent R_a during most of the machining. However, no significant changes were observed depending on the cutting conditions.
Saleem and Mumtaz [130]	Milling INCONEL® 625	Level 1 $v_c = 35$ m/min $f = 0.08$ mm/rev $a_p = 0.25$ mm Level 2 $v_c = 45$ m/min $f = 0.2$ mm/rev $a_p = 0.5$ mm	The Taguchi L ₈ array method was used in the analysis. a_p is found to be the statistically significant parameter for tool life with a 95% confidence level. Tool life is most affected by a_p followed by f_z with percentile contributions (PCR) of 45.43% and 18.425%, respectively, with lower values of the parameters resulting in better performance in general. A maximum tool life of 42.8 min was achieved when machining was done employing $f_z = 0.08$ mm/tooth and $a_p = 0.25$ mm with $v_c = 45$ m/min. A SEM analysis indicates adhesion, BUE, attrition and chipping to be the main wear mechanism in general.

4. Discussion

After all that has been presented throughout this paper, a SWOT analysis was performed to discuss present perceptions of the INCONEL[®] machinability (Table 13), tool-wear (Table 14) and coatings utility to the tools (Table 15).

Table 13. SWOT analysis about INCONEL[®] machinability.

Positive Factors		Negative Factors
Internal factors	Strengths Components with creep resistance in high-temperature operation.	Weakness Residual stress, Microhardness, Poor R_a , High F_c .
	Opportunities Making use of new non-conventional processes that improve machinability, like EDM and additive manufacturing (AM). Automobile industry and turbine blade manufacturing.	Threats Machining cost-effectiveness due to high t and TW.

Table 14. SWOT analysis of TW resultant from INCONEL[®] machining.

Positive Factors		Negative Factors
Internal factors	Strengths PcBN, carbide tools, ceramics and cermets can withstand high-temperature machining	Weakness Hardness drops with T rising.
	Opportunities With laser assistance, hBN has better lubricity, lower hardness, and higher tenacity than cBN.	Threats BUE, Abrasion, Adhesion, Debonding, Diffusion, Oxidation.

Table 15. SWOT analysis about cutting tools coatings.

Positive Factors		Negative Factors
Internal factors	Strengths Coatings prolong the effective tool's life.	Weakness Hardness drops with T rising. After a while, the coating starts to debond from the substrate
	Opportunities New coatings with better lubricity are being researched and developed (R&D'd).	Threats Some high-temperature applications with INCONEL [®] are not justifiable. Preference for uncoated PcBN tools. BUE, Abrasion, Adhesion, Debonding, Diffusion, Oxidation.

5. Conclusions

Despite significant progress in the traditional cutting tool technologies, the machining of INCONEL[®] 718 and 625 is still considered a great challenge because of the intrinsic characteristics of those Ni-superalloys. It is notable, nevertheless, that there has been a

pursuit to bring ease to conventional processes, resulting from the evolution of techniques and tool materials, to get better machinability with the Ni-based superalloys. From another point of view, by introducing non-conventional processes and assists like EDM, and hybrid techniques such as LAM and UAT, the evolution differential has a great potential to bring down manufacturing costs. Likewise, the conventional processes have had several improvements in the last five years, as reviewed along all states of the art, calling upon Taguchi DOE methods for improving tool-wear and for improving R_a , either with a lubrication environment or not. This is important for the own component's wear resistance. A constructive criticism is made of the usage of TGRA and DOE methods, which were several times noticed to be used by different research in the states of the art of this paper. It is efficient to take advantage of such powerful methods to evaluate a series of parameters in an L_x array, and through the combination between them, to achieve the best result of R_a . Nonetheless, it is known that one of the main challenges in tackling INCONEL[®] machining is the high costs of the manufacturing processes, due to the elapsed time milling, and turning, and this key factor has been neglected. With this review paper, it is suggested to the forthcoming authors to take advantage of TGRA and ANOVA analyses, concerning the achievement of low-cost solutions when machining INCONEL[®], at the same time quality is preserved by taking R_a parameter into account as it has been done so far. The present work highlighted a large amount of information regarding INCONEL[®] 718 traditional machining and applications, within the academic and scientific community, compared to its counterpart INCONEL[®] 625. On the other hand, the INCONEL[®] 625 showed advancements in non-conventional processes due to difficulties at the onset of chip cutting. Henceforward, research work is planned with the prospect of delivering a review paper regarding the evolution of lubrication environments, allied to the traditional machining of INCONEL[®].

Author Contributions: Conceptualization: A.F.V.P., F.J.G.S. and R.D.S.G.C.; methodology: A.F.V.P., F.J.G.S. and R.D.S.G.C.; validation: V.F.C.S., N.P.V.S. and A.M.P.J.; formal analysis: F.J.G.S., V.F.C.S. and R.C.M.S.-C.; investigation: A.F.V.P.; data curation: F.J.G.S., R.C.M.S.-C. and A.M.P.J.; writing—original draft preparation: A.F.V.P.; writing—review and editing: V.F.C.S., F.J.G.S., R.D.S.G.C. and R.C.M.S.-C.; visualization: R.C.M.S.-C. and A.M.P.J.; supervision: F.J.G.S. and R.D.S.G.C.; project administration: F.J.G.S.; funding acquisition: F.J.G.S. All authors have read and agreed to the published version of the manuscript.

Funding: The work is developed under the “DRIVOLUTION—Transition to the factory of the future”, with the reference DRIVOLUTION/BL/01/2023 research project, supported by European Structural and Investments Funds with the “Portugal2020” program scope.

Data Availability Statement: No new data was created.

Acknowledgments: The authors thank ISEP and INEGI for their support.

Conflicts of Interest: The authors declare no conflict of interest.

References

1. Ghiban, B.; Elefterie, C.F.; Guragata, C.; Bran, D. Requirements of Inconel 718 alloy for aeronautical applications. *AIP Conf. Proc.* **2018**, *1932*, 030016. [CrossRef]
2. Qadri, S.; Harmain, G.; Wani, M. Influence of Tool Tip Temperature on Crater Wear of Ceramic Inserts During Turning Process of Inconel-718 at Varying Hardness. *Tribol. Ind.* **2020**, *42*, 310–326. [CrossRef]
3. Nomoto, H. Development in materials for ultra-supercritical and advanced ultra-supercritical steam turbines. In *Advances in Steam Turbines for Modern Power Plants*, 2nd ed.; Chapter 13; Tanuma, T., Ed.; Woodhead Publishing: Sawston, UK, 2022; pp. 309–327.
4. Ghosh, R.N. Creep Life Predictions of Engineering Components: Problems & Prospects. *Procedia Eng.* **2013**, *55*, 599–606. [CrossRef]
5. Kassner, M.E. Chapter 10—Creep Fracture. In *Fundamentals of Creep in Metals and Alloys*, 3rd ed.; Kassner, M.E., Ed.; Butterworth-Heinemann: Boston, MA, USA, 2015; pp. 233–260.
6. Kassner, M.E. Chapter 11— γ/γ' Nickel-Based Superalloys. In *Fundamentals of Creep in Metals and Alloys*, 3rd ed.; Kassner, M.E., Ed.; Butterworth-Heinemann: Boston, MA, USA, 2015; pp. 261–273.
7. Weber, J.H.; Banerjee, M.K. Nickel and Nickel Alloys: An Overview. In *Reference Module in Materials Science and Materials Engineering*; Elsevier: Amsterdam, The Netherlands, 2019.
8. Liu, L.; Zhang, J.; Ai, C. Nickel-Based Superalloys. In *Encyclopedia of Materials: Metals and Alloys*; Caballero, F.G., Ed.; Elsevier: Oxford, UK, 2022; pp. 294–304.

9. Ashby, M.F. *Materials Selection in Mechanical Design*; Elsevier Science: Amsterdão, Países Baixos, 2016.
10. International Nickel Company. *Monel, Inconel, Nickel, and Nickel Alloys*; International Nickel Company: Toronto, ON, Canada, 1947.
11. Dai, H.; Shi, S.; Yang, L.; Hu, J.; Liu, C.; Guo, C.; Chen, X. Effects of elemental composition and microstructure inhomogeneity on the corrosion behavior of nickel-based alloys in hydrofluoric acid solution. *Corros. Sci.* **2020**, *176*, 108917. [\[CrossRef\]](#)
12. Deng, D. Additively Manufactured Inconel 718: Microstructures and Mechanical Properties. Licentiate Thesis, Comprehensive Summary. Linköping University Electronic Press, Linköping, Sweden, 2018.
13. Joshi, G.R.; Badheka, V.J.; Darji, R.S.; Oza, A.D.; Pathak, V.J.; Burduhos-Nergis, D.D.; Burduhos-Nergis, D.P.; Narwade, G.; Thirunavukarasu, G. The Joining of Copper to Stainless Steel by Solid-State Welding Processes: A Review. *Materials* **2022**, *15*, 7234. [\[CrossRef\]](#)
14. Wei, C.; Wang, Z.; Chen, J. Sulfuration corrosion failure analysis of Inconel 600 alloy heater sleeve in high-temperature flue gas. *Eng. Fail. Anal.* **2022**, *135*, 106111. [\[CrossRef\]](#)
15. Xu, D.; Guo, S. Chapter 2—Corrosion Types and Elemental Effects of Ni-Based and FeCrAl Alloys. In *Corrosion Characteristics, Mechanisms and Control Methods of Candidate Alloys in Sub- and Supercritical Water*; Xu, D., Guo, S., Eds.; Springer: Singapore, 2022; pp. 23–49.
16. Vinod, K.; Udaya Ravi, M.; Yuvaraja, N. A Study of Surface Morphology and Wear Rate Prediction of Coated Inconel 600, 625 and 718 Specimens. *Int. J. Sci. Acad. Res. (IJSAR)* **2023**, *3*, 1–9. [\[CrossRef\]](#)
17. Dhananchezian, M. Influence of variation in cutting velocity on temperature, surface finish, chip form and insert after dry turning Inconel 600 with TiAlN carbide insert. *Mater. Today Proc.* **2021**, *46*, 8271–8274. [\[CrossRef\]](#)
18. Mahesh, K.; Philip, J.T.; Joshi, S.N.; Kuriachen, B. Machinability of Inconel 718: A critical review on the impact of cutting temperatures. *Mater. Manuf. Process.* **2021**, *36*, 753–791. [\[CrossRef\]](#)
19. Yin, Q.; Liu, Z.; Wang, B.; Song, Q.; Cai, Y. Recent progress of machinability and surface integrity for mechanical machining Inconel 718: A review. *Int. J. Adv. Manuf. Technol.* **2020**, *109*, 215–245. [\[CrossRef\]](#)
20. Singh, N.; Routara, B.C.; Nayak, R.K. Study of machining characteristics of Inconel 601 with cryogenic cooled electrode in EDM using RSM. *Mater. Today Proc.* **2018**, *5*, 24277–24286. [\[CrossRef\]](#)
21. Harish, U.; Mruthunjaya, M.; Yogesha, K.; Siddappa, P.; Anil, K.K. Enhancing the performance of inconel 601 alloy by erosion resistant WC-CR-CO coated material. *J. Eng. Sci. Technol.* **2022**, *17*, 0379–0390.
22. Singh, J.B. Physical Metallurgy of Alloy 625. In *Alloy 625: Microstructure, Properties and Performance*; Chapter 3; Singh, J.B., Ed.; Springer Nature: Singapore, 2022; pp. 67–110.
23. Waghmode, S.P.; Dabade, U.A. Optimization of process parameters during turning of Inconel 625. *Mater. Today Proc.* **2019**, *19*, 823–826. [\[CrossRef\]](#)
24. Singh, J.B. Chapter 7—Corrosion Behavior of Alloy 625. In *Alloy 625: Microstructure, Properties and Performance*; Singh, J.B., Ed.; Springer Nature: Singapore, 2022; pp. 241–291.
25. Kosaraju, S.; Vijay Kumar, M.; Sateesh, N. Optimization of Machining Parameter in Turning Inconel 625. *Mater. Today Proc.* **2018**, *5*, 5343–5348. [\[CrossRef\]](#)
26. Singh, J.B. Chapter 1—Introduction. In *Alloy 625: Microstructure, Properties and Performance*; Singh, J.B., Ed.; Springer Nature: Singapore, 2022; pp. 1–27.
27. Yin, M.; Shao, Y.; Kang, X.; Long, J.; Zhang, X. Fretting corrosion behavior of WC-10Co-4Cr coating on Inconel 690 alloy by HVOF thermal spraying. *Tribol. Int.* **2023**, *177*, 107975. [\[CrossRef\]](#)
28. Zhang, Q.; Zhang, J.; Zhuang, Y.; Lu, J.; Yao, J. Hot Corrosion and Mechanical Performance of Repaired Inconel 718 Components via Laser Additive Manufacturing. *Materials* **2020**, *13*, 2128. [\[CrossRef\]](#)
29. Ding, J.; Xue, S.; Shang, Z.; Li, J.; Zhang, Y.; Su, R.; Niu, T.; Wang, H.; Zhang, X. Characterization of precipitation in gradient Inconel 718 superalloy. *Mater. Sci. Eng. A* **2021**, *804*, 140718. [\[CrossRef\]](#)
30. Teixeira, Ó.; Silva, F.J.G.; Atzeni, E. Residual stresses and heat treatments of Inconel 718 parts manufactured via metal laser beam powder bed fusion: An overview. *Int. J. Adv. Manuf. Technol.* **2021**, *113*, 3139–3162. [\[CrossRef\]](#)
31. Montazeri, S.; Aramesh, M.; Veldhuis, S.C. Novel application of ultra-soft and lubricious materials for cutting tool protection and enhancement of machining induced surface integrity of Inconel 718. *J. Manuf. Process.* **2020**, *57*, 431–443. [\[CrossRef\]](#)
32. Manikandan, S.G.K.; Sivakumar, D.; Kamaraj, M. 1—Physical metallurgy of alloy 718. In *Welding the Inconel 718 Superalloy*; Manikandan, S.G.K., Sivakumar, D., Kamaraj, M., Eds.; Elsevier: Amsterdam, The Netherlands, 2019; pp. 1–19.
33. Fayed, E.M.; Saadati, M.; Shahriari, D.; Brailovski, V.; Jahazi, M.; Medraj, M. Optimization of the Post-Process Heat Treatment of Inconel 718 Superalloy Fabricated by Laser Powder Bed Fusion Process. *Metals* **2021**, *11*, 144. [\[CrossRef\]](#)
34. Jeyapandiarajan, P.; Anthony, X.M. Evaluating the Machinability of Inconel 718 under Different Machining Conditions. *Procedia Manuf.* **2019**, *30*, 253–260. [\[CrossRef\]](#)
35. Pröbstle, M.; Neumeier, S.; Hopfenmüller, J.; Freund, L.P.; Niendorf, T.; Schwarze, D.; Göken, M. Superior creep strength of a nickel-based superalloy produced by selective laser melting. *Mater. Sci. Eng. A* **2016**, *674*, 299–307. [\[CrossRef\]](#)
36. Evans, R. 2—Selection and testing of metalworking fluids. In *Metalworking Fluids (MWFs) for Cutting and Grinding*; Astakhov, V.P., Joksche, S., Eds.; Woodhead Publishing: Sawston, UK, 2012; pp. 23–78.
37. Wang, C.; Ming, W.; Chen, M. Milling tool's flank wear prediction by temperature dependent wear mechanism determination when machining Inconel 182 overlays. *Tribol. Int.* **2016**, *104*, 140–156. [\[CrossRef\]](#)

38. Zhang, P.; Li, J.; Yu, H.L.; Tu, X.H.; Li, W. An experimental study on the fretting wear behavior of Inconel 600 and 690 in pure water. *Wear* **2021**, 486–487, 203995. [\[CrossRef\]](#)
39. Mohapatra, S.; Rahul; Kumar Sahoo, A. Comparative study of Inconel 601, 625, 718, 825 super-alloys during Electro-Discharge Machining. *Mater. Today Proc.* **2022**, 56, 226–230. [\[CrossRef\]](#)
40. Liu, X.; Fan, J.; Cao, K.; Chen, F.; Yuan, R.; Liu, D.; Tang, B.; Kou, H.; Li, J. Creep anisotropy behavior, deformation mechanism, and its efficient suppression method in Inconel 625 superalloy. *J. Mater. Sci. Technol.* **2023**, 133, 58–76. [\[CrossRef\]](#)
41. Kurniawan, R.; Park, G.C.; Park, K.M.; Zhen, Y.; Kwak, Y.I.; Kim, M.C.; Lee, J.M.; Ko, T.J.; Park, C.-S. Machinability of modified Inconel 713C using a WC TiAlN-coated tool. *J. Manuf. Process.* **2020**, 57, 409–430. [\[CrossRef\]](#)
42. Tanaka, H.; Sugihara, T.; Enomoto, T. High Speed Machining of Inconel 718 Focusing on Wear Behaviors of PCBN Cutting Tool. *Procedia CIRP* **2016**, 46, 545–548. [\[CrossRef\]](#)
43. Şirin, Ş.; Kivak, T. Effects of hybrid nanofluids on machining performance in MQL-milling of Inconel X-750 superalloy. *J. Manuf. Process.* **2021**, 70, 163–176. [\[CrossRef\]](#)
44. Gupta, M.K.; Song, Q.; Liu, Z.; Sarikaya, M.; Jamil, M.; Mia, M.; Singla, A.K.; Khan, A.M.; Khanna, N.; Pimenov, D.Y. Environment and economic burden of sustainable cooling/lubrication methods in machining of Inconel-800. *J. Clean. Prod.* **2021**, 287, 125074. [\[CrossRef\]](#)
45. Yadav, R.K.; Abhishek, K.; Mahapatra, S.S.; Nandi, G. A study on machinability aspects and parametric optimization of Inconel 825 using Rao1, Rao2, Rao3 approach. *Mater. Today Proc.* **2021**, 47, 2784–2789. [\[CrossRef\]](#)
46. ASTM Standard B637-16; Standard Specification for Precipitation-Hardening and Cold Worked Nickel Alloy Bars, Forgings, and Forging Stock for Moderate or High Temperature Service. ASTM International: West Conshohocken, PA, USA, 2016; Volume 7. [\[CrossRef\]](#)
47. Astakhov, V.P.; Godlevskiy, V. 3—Delivery of metalworking fluids in the machining zone. In *Metalworking Fluids (MWFs) for Cutting and Grinding*; Astakhov, V.P., Joks, S., Eds.; Woodhead Publishing: Sawston, UK, 2012; pp. 79–134.
48. Soffel, F.; Eisenbarth, D.; Hosseini, E.; Wegener, K. Interface strength and mechanical properties of Inconel 718 processed sequentially by casting, milling, and direct metal deposition. *J. Mater. Process. Technol.* **2021**, 291, 117021. [\[CrossRef\]](#)
49. Sierra-Soraluce, A.; Li, G.; Santofimia, M.J.; Molina-Aldareguia, J.M.; Smith, A.; Muratori, M.; Sabirov, I. Effect of microstructure on tensile properties of quenched and partitioned martensitic stainless steels. *Mater. Sci. Eng. A* **2023**, 864, 144540. [\[CrossRef\]](#)
50. Ding, H.; Zou, B.; Wang, X.; Liu, J.; Li, L. Microstructure, mechanical properties and machinability of 316L stainless steel fabricated by direct energy deposition. *Int. J. Mech. Sci.* **2023**, 243, 108046. [\[CrossRef\]](#)
51. Danish, M.; Ginta, T.L.; Yasir, M.; Rani AM, A. Chapter 1—Light alloys and their machinability. In *Machining of Light Alloys: Aluminum, Titanium, and Magnesium*; Carou, D., Davim, J., Eds.; Academic Press: Cambridge, MA, USA, 2018.
52. Kumar Wagri, N.; Petare, A.; Agrawal, A.; Rai, R.; Malviya, R.; Dohare, S.; Kishore, K. An overview of the machinability of alloy steel. *Mater. Today Proc.* **2022**, 62, 3771–3781. [\[CrossRef\]](#)
53. Zhao, J.; Liu, Z.; Wang, B.; Hu, J. PVD AlTiN coating effects on tool-chip heat partition coefficient and cutting temperature rise in orthogonal cutting Inconel 718. *Int. J. Heat Mass Transf.* **2020**, 163, 120449. [\[CrossRef\]](#)
54. Loewen, E.G.; Shaw, M.C. On the Analysis of Cutting-Tool Temperatures. *Trans. Am. Soc. Mech. Eng.* **2022**, 76, 217–225. [\[CrossRef\]](#)
55. Shaw, M.C.; Cookson, J. *Metal Cutting Principles*; Oxford University Press: New York, NY, USA, 2005; Volume 2.
56. Kato, T.; Fujii, H. Energy Partition in Conventional Surface Grinding. *J. Manuf. Sci. Eng.* **1999**, 121, 393–398. [\[CrossRef\]](#)
57. List, G.; Sutter, G.; Bouthiche, A. Cutting temperature prediction in high speed machining by numerical modelling of chip formation and its dependence with crater wear. *Int. J. Mach. Tools Manuf.* **2012**, 54–55, 1–9. [\[CrossRef\]](#)
58. Gecim, B.; Winer, W.O. Transient Temperatures in the Vicinity of an Asperity Contact. *J. Tribol.* **1985**, 107, 333–341. [\[CrossRef\]](#)
59. Reznikov, A.; Reznikov, A. Thermophysical aspects of metal cutting processes. *Mashinostroenie Mosc.* **1981**, 212.
60. Grzesik, W. *Advanced Machining Processes of Metallic Materials: Theory, Modelling and Applications*; Elsevier: Amsterdam, The Netherlands, 2008.
61. Andresen, P.L. 5—Understanding and predicting stress corrosion cracking (SCC) in hot water. In *Stress Corrosion Cracking of Nickel Based Alloys in Water-Cooled Nuclear Reactors*; Féron, D., Staehle, R.W., Eds.; Woodhead Publishing: Sawston, UK, 2016; pp. 169–238.
62. Féron, D.; Guerre, C.; Herms, E.; Laghoutaris, P. 9—Stress corrosion cracking of Alloy 600: Overviews and experimental techniques. In *Stress Corrosion Cracking of Nickel Based Alloys in Water-Cooled Nuclear Reactors*; Féron, D., Staehle, R.W., Eds.; Woodhead Publishing: Sawston, UK, 2016; pp. 325–353.
63. Dai, X.; Zhuang, K.; Pu, D.; Zhang, W.; Ding, H. An Investigation of the Work Hardening Behavior in Interrupted Cutting Inconel 718 under Cryogenic Conditions. *Materials* **2020**, 13, 2202. [\[CrossRef\]](#) [\[PubMed\]](#)
64. Guimaraes, M.C.R.; Fogagnolo, J.B.; Paiva, J.M.; Veldhuis, S.C.; Diniz, A.E. Evaluation of milling parameters on the surface integrity of welded inconel 625. *J. Mater. Res. Technol.* **2022**, 20, 2611–2628. [\[CrossRef\]](#)
65. Li, X.; Liu, X.; Yue, C.; Liang, S.Y.; Wang, L. Systematic review on tool breakage monitoring techniques in machining operations. *Int. J. Mach. Tools Manuf.* **2022**, 176, 103882. [\[CrossRef\]](#)
66. Zheng, H.; Liu, K. Machinability of Engineering Materials. In *Handbook of Manufacturing Engineering and Technology*; Nee, A., Ed.; Springer London: London, UK, 2013; pp. 1–34.
67. Wang, Z.; Kovvuri, V.; Araujo, A.; Bacci, M.; Hung, W.N.P.; Bukkapatnam, S.T.S. Built-up-edge effects on surface deterioration in micromilling processes. *J. Manuf. Process.* **2016**, 24, 321–327. [\[CrossRef\]](#)

68. Nouari, M.; Haddag, B.; Moufki, A.; Atlati, S. Chapter 2—Investigation on the built-up edge process when dry machining aeronautical aluminum alloys. In *Machining of Light Alloys: Aluminum, Titanium, and Magnesium*; Carou, D., Davim, J., Eds.; Academic Press: Cambridge, MA, USA, 2018.
69. Bartolomeis, A.D.; Newman, S.T.; Shokrani, A. Initial investigation on Surface Integrity when Machining Inconel 718 with Conventional and Electrostatic Lubrication. *Procedia CIRP* **2020**, *87*, 65–70. [\[CrossRef\]](#)
70. Anburaj, R.; Pradeep Kumar, M. Experimental studies on cryogenic CO₂ face milling of Inconel 625 superalloy. *Mater. Manuf. Process.* **2021**, *36*, 814–826. [\[CrossRef\]](#)
71. Lakner, T.; Hardt, M. A Novel Experimental Test Bench to Investigate the Effects of Cutting Fluids on the Frictional Conditions in Metal Cutting. *J. Manuf. Mater. Process.* **2020**, *4*, 45. [\[CrossRef\]](#)
72. Bonnet, C.; Valiorgue, F.; Rech, J.; Claudin, C.; Hamdi, H.; Bergheau, J.M.; Gilles, P. Identification of a friction model—Application to the context of dry cutting of an AISI 316L austenitic stainless steel with a TiN coated carbide tool. *Int. J. Mach. Tools Manuf.* **2008**, *48*, 1211–1223. [\[CrossRef\]](#)
73. Kuzu, A.T.; Berenji, K.R.; Ekim, B.C.; Bakkal, M. The thermal modeling of deep-hole drilling process under MQL condition. *J. Manuf. Process.* **2017**, *29*, 194–203. [\[CrossRef\]](#)
74. Kim, E.J.; Lee, C.M. A Study on the Optimal Machining Parameters of the Induction Assisted Milling with Inconel 718. *Materials* **2019**, *12*, 233. [\[CrossRef\]](#) [\[PubMed\]](#)
75. Vignesh, M.; Ramanujam, R. Chapter 9—Laser-assisted high speed machining of Inconel 718 alloy. In *High Speed Machining*; Gupta, K., Paulo Davim, J., Eds.; Academic Press: Cambridge, MA, USA, 2020; pp. 243–262.
76. Okafor, A.C. Chapter 5—Cooling and machining strategies for high speed milling of titanium and nickel super alloys. In *High Speed Machining*; Gupta, K., Paulo Davim, J., Eds.; Academic Press: Cambridge, MA, USA, 2020; pp. 127–161.
77. Hadi, M.A.; Ghani, J.A.; Haron, C.H.C.; Kasim, M.S. Comparison between Up-milling and Down-milling Operations on Tool Wear in Milling Inconel 718. *Procedia Eng.* **2013**, *68*, 647–653. [\[CrossRef\]](#)
78. Bo, P.; Fan, H.; Bartoň, M. Efficient 5-axis CNC trochoidal flank milling of 3D cavities using custom-shaped cutting tools. *Comput.-Aided Des.* **2022**, *151*, 103334. [\[CrossRef\]](#)
79. Liu, D.; Zhang, Y.; Luo, M.; Zhang, D. Investigation of Tool Wear and Chip Morphology in Dry Trochoidal Milling of Titanium Alloy Ti-6Al-4V. *Materials* **2019**, *12*, 1937. [\[CrossRef\]](#)
80. Pleta, A.; Nithyanand, G.; Niaki, F.A.; Mears, L. Identification of optimal machining parameters in trochoidal milling of Inconel 718 for minimal force and tool wear and investigation of corresponding effects on machining affected zone depth. *J. Manuf. Process.* **2019**, *43*, 54–62. [\[CrossRef\]](#)
81. Shankar, S.; Mohanraj, T.; Pramanik, A. Tool Condition Monitoring While Using Vegetable Based Cutting Fluids during Milling of Inconel 625. *J. Adv. Manuf. Syst.* **2019**, *18*, 563–581. [\[CrossRef\]](#)
82. Alonso, U.; Veiga, F.; Suárez, A.; Gil Del Val, A. Characterization of Inconel 718®superalloy fabricated by wire Arc Additive Manufacturing: Effect on mechanical properties and machinability. *J. Mater. Res. Technol.* **2021**, *14*, 2665–2676. [\[CrossRef\]](#)
83. Boozarpoor, M.; Teimouri, R.; Yazdani, K. Comprehensive study on effect of orthogonal turn-milling parameters on surface integrity of Inconel 718 considering production rate as constrain. *Int. J. Lightweight Mater. Manuf.* **2021**, *4*, 145–155. [\[CrossRef\]](#)
84. Amigo, F.J.; Urbikain, G.; Pereira, O.; Fernández-Lucio, P.; Fernández-Valdivielso, A.; de Lacalle, L.N.L. Combination of high feed turning with cryogenic cooling on Haynes 263 and Inconel 718 superalloys. *J. Manuf. Process.* **2020**, *58*, 208–222. [\[CrossRef\]](#)
85. Raykar, S.J.; Chaugule, Y.G.; Pasare, V.I.; Sawant, D.A.; Patil, U.N. Analysis of microhardness and degree of work hardening (DWH) while turning Inconel 718 with high pressure coolant environment. *Mater. Today Proc.* **2022**, *59*, 1088–1093. [\[CrossRef\]](#)
86. Infante-García, D.; Diaz-Álvarez, J.; Cantero, J.-L.; Muñoz-Sánchez, A.; Miguélez, M.-H. Influence of the undeformed chip cross section in finishing turning of Inconel 718 with PCBN tools. *Procedia CIRP* **2018**, *77*, 122–125. [\[CrossRef\]](#)
87. Meyer, R.; Köhler, J.; Denkena, B. Influence of the tool corner radius on the tool wear and process forces during hard turning. *Int. J. Adv. Manuf. Technol.* **2012**, *58*, 933–940. [\[CrossRef\]](#)
88. Makhesana, M.A.; Patel, K.M.; Krolczyk, G.M.; Danish, M.; Singla, A.K.; Khanna, N. Influence of MoS₂ and graphite-reinforced nanofluid-MQL on surface roughness, tool wear, cutting temperature and microhardness in machining of Inconel 625. *CIRP J. Manuf. Sci. Technol.* **2023**, *41*, 225–238. [\[CrossRef\]](#)
89. Airao, J.; Nirala, C.K.; Khanna, N. Novel use of ultrasonic-assisted turning in conjunction with cryogenic and lubrication techniques to analyze the machinability of Inconel 718. *J. Manuf. Process.* **2022**, *81*, 962–975. [\[CrossRef\]](#)
90. Venkatesan, K.; Nagendra, K.U.; Anudeep, C.M.; Cotton, A.E. Experimental Investigation and Parametric Optimization on Hole Quality Assessment During Micro-drilling of Inconel 625 Superalloy. *Arab. J. Sci. Eng.* **2021**, *46*, 2283–2309. [\[CrossRef\]](#)
91. Cherrared, D. Numerical simulation of film cooling a turbine blade through a row of holes. *J. Therm. Eng.* **2017**, *3*, 1110. [\[CrossRef\]](#)
92. Neo, D.W.K.; Liu, K.; Kumar, A.S. High throughput deep-hole drilling of Inconel 718 using PCBN gun drill. *J. Manuf. Process.* **2020**, *57*, 302–311. [\[CrossRef\]](#)
93. Sahoo, A.K.; Jeet, S.; Bagal, D.K.; Barua, A.; Pattanaik, A.K.; Behera, N. Parametric optimization of CNC-drilling of Inconel 718 with cryogenically treated drill-bit using Taguchi-Whale optimization algorithm. *Mater. Today Proc.* **2022**, *50*, 1591–1598. [\[CrossRef\]](#)
94. Ratnam, C.; Adarsha Kumar, K.; Murthy, B.S.N.; Venkata Rao, K. An experimental study on boring of Inconel 718 and multi response optimization of machining parameters using Response Surface Methodology. *Mater. Today Proc.* **2018**, *5*, 27123–27129. [\[CrossRef\]](#)

95. Liu, L.; Thangaraj, M.; Karmiris-Obratański, P.; Zhou, Y.; Annamalai, R.; Machnik, R.; Elsheikh, A.; Markopoulos, A.P. Optimization of Wire EDM Process Parameters on Cutting Inconel 718 Alloy with Zinc-Diffused Coating Brass Wire Electrode Using Taguchi-DEAR Technique. *Coatings* **2022**, *12*, 1612. [\[CrossRef\]](#)
96. Kliuev, M.; Kutin, A.; Wegener, K. Electrode wear pattern during EDM milling of Inconel 718. *Int. J. Adv. Manuf. Technol.* **2021**, *117*, 2369–2375. [\[CrossRef\]](#)
97. Manikandan, N.; Binoj, J.S.; Thejasree, P.; Sasikala, P.; Anusha, P. Application of Taguchi method on Wire Electrical Discharge Machining of Inconel 625. *Mater. Today Proc.* **2021**, *39*, 121–125. [\[CrossRef\]](#)
98. Hussain, A.; Kumar Sharma, A.; Preet Singh, J. Maximizing MRR of Inconel 625 machining through process parameter optimization of EDM. *Mater. Today Proc.* **2022**; *In Press*. [\[CrossRef\]](#)
99. Rahul; Datta, S.; Biswal, B.B.; Mahapatra, S.S. Machinability analysis of Inconel 601, 625, 718 and 825 during electro-discharge machining: On evaluation of optimal parameters setting. *Measurement* **2019**, *137*, 382–400. [\[CrossRef\]](#)
100. Farooq, M.U.; Anwar, S.; Kumar, M.S.; AlFaify, A.; Ali, M.A.; Kumar, R.; Haber, R. A Novel Flushing Mechanism to Minimize Roughness and Dimensional Errors during Wire Electric Discharge Machining of Complex Profiles on Inconel 718. *Materials* **2022**, *15*, 7330. [\[CrossRef\]](#)
101. ISO 8688-2:1989(E); Tool Life Testing in Milling—Part 2: End milling. ISO: London, UK, 1989; 26p.
102. ISO 3685:1993(E); Tool-Life Testing with Single-Point Turning Tools. ISO: London, UK, 1993; 53p.
103. Zhang, X.; Peng, Z.; Liu, L.; Zhang, X. A Tool Life Prediction Model Based on Taylor's Equation for High-Speed Ultrasonic Vibration Cutting Ti and Ni Alloys. *Coatings* **2022**, *12*, 1553. [\[CrossRef\]](#)
104. Archard, J.F. Contact and Rubbing of Flat Surfaces. *J. Appl. Phys.* **1953**, *24*, 981–988. [\[CrossRef\]](#)
105. Usui, E.; Shirakashi, T.; Kitagawa, T. Analytical Prediction of Three Dimensional Cutting Process—Part 3: Cutting Temperature and Crater Wear of Carbide Tool. *J. Eng. Ind.* **1978**, *100*, 236–243. [\[CrossRef\]](#)
106. Usui, E.; Shirakashi, T.; Kitagawa, T. Analytical prediction of cutting tool wear. *Wear* **1984**, *100*, 129–151. [\[CrossRef\]](#)
107. Takeyama, H.; Murata, R. Basic Investigation of Tool Wear. *J. Eng. Ind.* **1963**, *85*, 33–37. [\[CrossRef\]](#)
108. Childs, T.H.C.; Maekawa, K.; Obikawa, T.; Yamane, Y. *Metal Machining: Theory and Applications*; Arnold: London, UK, 2000.
109. Schmidt, C.; Frank, P.; Weule, H.; Schmidt, J.; Yen, Y.; Altan, T. Tool wear prediction and verification in orthogonal cutting. In Proceedings of the 6th CIRP Workshop on Modeling of Machining, Hamilton, ON, Canada, 19–20 May 2003; pp. 93–100.
110. Luo, X.; Cheng, K.; Holt, R.; Liu, X. Modeling flank wear of carbide tool insert in metal cutting. *Wear* **2005**, *259*, 1235–1240. [\[CrossRef\]](#)
111. Astakhov, V.P. Effects of the cutting feed, depth of cut, and workpiece (bore) diameter on the tool wear rate. *Int. J. Adv. Manuf. Technol.* **2007**, *34*, 631–640. [\[CrossRef\]](#)
112. Astakhov, V.P. Chapter 4 Cutting tool wear, tool life and cutting tool physical resource. In *Tribology and Interface Engineering Series*; Briscoe, B.J., Ed.; Elsevier: Amsterdam, The Netherlands, 2006; Volume 52, pp. 220–275.
113. Attanasio, A.; Ceretti, E.; Fiorentino, A.; Cappellini, C.; Giardini, C. Investigation and FEM-based simulation of tool wear in turning operations with uncoated carbide tools. *Wear* **2010**, *269*, 344–350. [\[CrossRef\]](#)
114. Attanasio, A.; Ceretti, E.; Rizzuti, S.; Umbrello, D.; Micari, F. 3D finite element analysis of tool wear in machining. *CIRP Ann.* **2008**, *57*, 61–64. [\[CrossRef\]](#)
115. Pálmai, Z. Proposal for a new theoretical model of the cutting tool's flank wear. *Wear* **2013**, *303*, 437–445. [\[CrossRef\]](#)
116. Halila, F.; Czarnota, C.; Nouari, M. A new abrasive wear law for the sticking and sliding contacts when machining metallic alloys. *Wear* **2014**, *315*, 125–135. [\[CrossRef\]](#)
117. Halila, F.; Czarnota, C.; Nouari, M. New stochastic wear law to predict the abrasive flank wear and tool life in machining process. *Proc. Inst. Mech. Eng. Part J. J. Eng. Tribol.* **2014**, *228*, 1243–1251. [\[CrossRef\]](#)
118. Wang, R.; Yang, D.; Wang, W.; Wei, F.; Lu, Y.; Li, Y. Tool Wear in Nickel-Based Superalloy Machining: An Overview. *Processes* **2022**, *10*, 2380. [\[CrossRef\]](#)
119. De Bartolomeis, A.; Newman, S.T.; Jawahir, I.S.; Biermann, D.; Shokrani, A. Future research directions in the machining of Inconel 718. *J. Mater. Process. Technol.* **2021**, *297*, 117260. [\[CrossRef\]](#)
120. Breidenstein, B.; Grove, T.; Krödel, A.; Sitab, R. Influence of hexagonal phase transformation in laser prepared PcBN cutting tools on tool wear in machining of Inconel 718. *Met. Powder Rep.* **2019**, *74*, 237–243. [\[CrossRef\]](#)
121. Rakesh, P.R.; Chakradhar, D. Machining performance comparison of Inconel 625 superalloy under sustainable machining environments. *J. Manuf. Process.* **2023**, *85*, 742–755. [\[CrossRef\]](#)
122. Hoier, P.; Malakizadi, A.; Krajnik, P.; Klement, U. Study of flank wear topography and surface-deformation of cemented carbide tools after turning Alloy 718. *Procedia CIRP* **2018**, *77*, 537–540. [\[CrossRef\]](#)
123. Sousa, V.F.C.; Silva, F.J.G. Recent Advances on Coated Milling Tool Technology—A Comprehensive Review. *Coatings* **2020**, *10*, 235. [\[CrossRef\]](#)
124. Sousa, V.F.C.; Da Silva, F.J.G.; Pinto, G.F.; Baptista, A.; Alexandre, R. Characteristics and Wear Mechanisms of TiAlN-Based Coatings for Machining Applications: A Comprehensive Review. *Metals* **2021**, *11*, 260. [\[CrossRef\]](#)
125. Jain, A.; Bajpai, V. Chapter 1—Introduction to high-speed machining (HSM). In *High Speed Machining*; Gupta, K., Paulo Davim, J., Eds.; Academic Press: Cambridge, MA, USA, 2020; pp. 1–25.
126. Montazeri, S.; Aramesh, M.; Rawal, S.; Veldhuis, S.C. Characterization and machining performance of a chipping resistant ultra-soft coating used for the machining of Inconel 718. *Wear* **2021**, *474–475*, 203759. [\[CrossRef\]](#)

127. Agarwal, A.; Potthoff, N.; Shah, A.M.; Mears, L.; Wiederkehr, P. Analyzing the evolution of tool wear area in trochoidal milling of Inconel 718 using image processing methodology. *Manuf. Lett.* **2022**, *33*, 373–379. [[CrossRef](#)]
128. Liu, E.; An, W.; Xu, Z.; Zhang, H. Experimental study of cutting-parameter and tool life reliability optimization in inconel 625 machining based on wear map approach. *J. Manuf. Process.* **2020**, *53*, 34–42. [[CrossRef](#)]
129. Criado, V.; Díaz-Álvarez, J.; Cantero, J.L.; Miguélez, M.H. Study of the performance of PCBN and carbide tools in finishing machining of Inconel 718 with cutting fluid at conventional pressures. *Procedia CIRP* **2018**, *77*, 634–637. [[CrossRef](#)]
130. Saleem, M.Q.; Mumtaz, S. Face milling of Inconel 625 via wiper inserts: Evaluation of tool life and workpiece surface integrity. *J. Manuf. Process.* **2020**, *56*, 322–336. [[CrossRef](#)]

Disclaimer/Publisher’s Note: The statements, opinions and data contained in all publications are solely those of the individual author(s) and contributor(s) and not of MDPI and/or the editor(s). MDPI and/or the editor(s) disclaim responsibility for any injury to people or property resulting from any ideas, methods, instructions or products referred to in the content.